

Setup of a Tunable, Narrowband, Continuous Wave Optical Parametric Oscillator at 606 nm

Aufbau eines durchstimmbaren, schmalbandigen, Dauerstrich optischen parametrischen Oszillators bei 606 nm

Masterarbeit von Benedikt Moneke

Tag der Einreichung: 3. September 2020

1. Gutachten: Prof. Dr. Thomas Halfmann

2. Gutachten: Markus Stabel, M.Sc.

Darmstadt



**TECHNISCHE
UNIVERSITÄT
DARMSTADT**

Fachbereich Physik
Institut für Angewandte
Physik
Nichtlineare Optik /
Quantenoptik

Setup of a Tunable, Narrowband, Continuous Wave Optical Parametric Oscillator at 606 nm

Aufbau eines durchstimmbaren, schmalbandigen, Dauerstrich optischen parametrischen Oszillators bei 606 nm

Masterarbeit von Benedikt Moneke

1. Gutachten: Prof. Dr. Thomas Halfmann
2. Gutachten: Markus Stabel, M.Sc.

Tag der Einreichung: 3. September 2020

Darmstadt

Contents

Introduction	1
1 The Nonlinear Laser System	3
1.1 Design of the Nonlinear Laser System	3
1.1.1 General Configuration of the Nonlinear Laser System	3
1.1.2 Cavity Design	7
1.1.3 Nonlinear Crystal Design	9
1.1.4 Etalon Design	14
1.1.5 Pump Injection Setup	15
1.2 Mounting Setup	16
1.2.1 Table Mounted Laser System	16
1.2.2 Adjustment of Optical Elements	18
1.2.3 Cavity Block	19
1.2.4 Acoustic Box	22
2 Characterization of the Laser System	23
2.1 Optical Parametric Oscillator Only	23
2.2 Optical Parametric Oscillation and Sum Frequency Generation	27
3 Reduction of Linewidth	32
3.1 Linewidth Measurement	32
3.2 General Setup and First Results	33
3.3 Linewidth of Seed and Amplifier	34
3.4 Influence of Sonic Waves	35
3.5 Linewidth of the Stabilized Laser System	37
3.5.1 Pound-Drever-Hall Stabilization	38
3.5.2 Stabilization Setup	39
3.5.3 Linewidth with the Active Stabilization	40
3.6 Comparison with the Current System	42
Conclusion and Outlook	45

Introduction

Distributed quantum computing and quantum communication networks require the exchange of quantum states. In order to decrease the transmission loss due to an increasing transmission distance, quantum repeaters can be used. If photons are used as information carriers, the quantum repeater needs a quantum memory to store them [1].

Our group implements quantum memories in rare earth doped crystals. We achieved storage times up to a minute in an yttrium orthosilicate crystal doped with the rare earth praseodymium (Pr:YSO) using **electromagnetically induced transparency (EIT)** [2]. We want to implement another storage protocol, **atomic frequency comb (AFC)**, because it offers a higher bandwidth, does not require a readout pulse which increases noise, and allows to store several photons at different moments independently of the optical depth [3]. An atomic frequency comb is a comb-like absorption spectrum. When a photon enters a medium with such a structure, it excites the atoms or ions of the individual absorption peaks creating atomic coherences. As every peak has a slightly different frequency, their phase evolution differs. Because of the periodic structure, they have the same phase again after the time $T = \frac{1}{\Delta}$, with the distance Δ between two adjacent absorption peaks. In this moment the atomic coherences couple efficiently to the light field again such that they emit the originally stored photon again.

Different ions in Pr:YSO experience different magnetic fields and Zeeman splittings, which causes an inhomogeneous broadening. Changing the state of some ions, they can be made to absorb or transmit at specific frequencies corresponding to that inhomogeneously broadened atomic transition and thus an AFC can be prepared by optical pumping. In order to change their state, the ions are optically excited and decay with a certain probability into the desired state [4]. The spectral precision of the optical excitement depends on the laser linewidth, therefore the linewidth limits the size of the smallest possible substructure and consequently the minimum peak width. That peak width in turn limits the number of peaks and achievable finesse of the comb in a given frequency range.

In order to increase the storage time, we want to use some techniques already used by Heinze *et al.* in their experiments with electromagnetically induced transparency [2]. One of those, ZEFOZ, uses an external magnetic field, at which the first order of the Zeeman shift vanishes, which reduces the negative effects of changes in the magnetic field, for example due to spontaneous spin flips. The induced Zeeman splitting, however, reduces the frequency range available for AFC to a few hundred kilohertz due to the more complicated level structure.

Our current light source, an optical parametric oscillator with intracavity sum frequency generation and Pound-Drever-Hall frequency stabilization [2], has a linewidth of 58 kHz over 86 ms [5]. That linewidth allows just three peaks in ZEFOZ conditions such that an AFC is just achievable. Furthermore, the AFC's

finesse can barely be changed and the storage efficiency cannot be optimized, because it depends strongly on the finesse [6].

The only solution for a higher finesse is a light source with a smaller linewidth. That is the goal of this work. Several attempts to reduce the linewidth of the current system, for example by changing its active stabilization, failed [5]. Now we focus on the possibility of improving the light source itself or exchanging it for a better one.

We set out to design and construct a coherent, continuous wave light source at 606 nm with at least 0.5 W output power and a linewidth as small as the current one or better. It is difficult to find a suitable light source. Nonlinear optics has offered successful solutions. Among those are our current system with optical parametric oscillation and sum frequency generation [7] and a similar system with optical parametric oscillation and second harmonic generation which achieves a linewidth below 1 kHz over 1 s [8]. Therefore, we continue this path of nonlinear optics in order to combine the performance of both systems, the right wavelength with a small linewidth. If the new system performs worse than the current one, it might, nevertheless, offer helpful clues in order to improve the current one or design a better version.

This thesis is structured as follows. The first chapter presents this first step, the design of the laser system. Its first section deals with the optical system and the second section with the mounting solution designed to reduce the linewidth. In the second chapter, the laser system is characterized and the results are compared to the requirements. Having built and characterized the laser system, we present in the third and last chapter the core quest for a small linewidth. There we present the measures tried in order to decrease the linewidth and a comparison with the current laser system.

Chapter 1

The Nonlinear Laser System

This chapter describes the design of the nonlinear laser system for coherent radiation at a wavelength of 606 nm. The sections describe the different parts of the design. The first section deals with the optical system itself, the second one deals with the mechanically stable mounting of the optical elements.

1.1 Design of the Nonlinear Laser System

The nonlinear laser system is geared towards light storage experiments in yttrium orthosilicate crystals doped with praseodymium (Pr:YSO), therefore its output has to fulfill the following requirements: It has to be coherent and continuous wave. The wavelength should be 605.98 nm with a tunability of at least 20 pm in each direction and the linewidth should be small. The currently used system has a linewidth of 58 kHz over 86 ms [5], which is insufficient for future experiments and, therefore, the goal is a smaller linewidth than those 58 kHz using an active stabilization. The output power should be above 0.5 W in order to have enough power for the light storage experiments.

1.1.1 General Configuration of the Nonlinear Laser System

The first design choice is the process which generates the output according to our requirements. Current laser diodes do not reach the required output power in continuous wave operation at 606 nm wavelength [9]. Praseodymium doped laser media do exist but their different host material changes the emission wavelength, for example the laser medium Pr:YLF emits light with more than 0.5 W, but at 604.1 nm or 606.9 nm, both just outside the desired wavelength [10]. Dye lasers offer the wavelength and power but not the linewidth, at least the commercially available *Matisse* product line by *Spectra Physics*, whose dye laser we used before [11].

Nonlinear optics offers the possibility to mix frequencies and thus emit light at a broad range of new wavelengths, including at 606 nm. Several processes can be combined as well. The first subsection deals with the nonlinear optics itself. The second subsection deals with the different possibilities how to achieve a setup meeting our requirements.

Nonlinear Optics

Nonlinear optics considers a nonlinear relationship between an electric field \vec{E} and the dielectric polarization \vec{P} of some matter caused by this electric field. Light as an electromagnetic wave contains an oscillating electric field. A power series expansion of the dielectric polarization is

$$\vec{P} = \epsilon_0 (\chi^{(1)} \odot \vec{E} + \chi^{(2)} \odot \vec{E} \odot \vec{E} + \chi^{(3)} \odot \vec{E} \odot \vec{E} \odot \vec{E} + \dots) \quad (1.1)$$

with the dielectric permeability of vacuum ϵ_0 and the electric susceptibility of n^{th} order $\chi^{(n)}$. The electric susceptibility is a tensor therefore the polarization is not necessarily parallel to the electric field. The electric susceptibility and the electric field are convoluted, which is expressed by the sign \odot [12].

The nonlinear dielectric susceptibilities are that small, that they can be neglected in many cases, even in a **nonlinear medium**, which is a medium with a relative high nonlinear susceptibility. For example, the nonlinear medium PPLN has only $25 \frac{\text{pm}}{\text{V}}$ as the highest component of its second order susceptibility, while its first order susceptibility is 3.4 [13]. Therefore, a very high electric field has to be present for a similar order of magnitude of the first and second order of polarization. Subsection 1.1.3 talks about further requirements than a high nonlinear susceptibility for an efficient application of a nonlinear medium.

If the electric field changes in time, the polarization changes as well. This is the case with the oscillating electric field of light, which causes an oscillating polarization. In the first order, the polarization oscillates with the same frequency as the electric field, because they are proportional. In the higher orders, different frequency components have to be taken into consideration. Let the matter be isotropic so that the vector character can be ignored, because \vec{P} is parallel to \vec{E} . And let $E_m^{(+)} = \frac{E_m}{2} e^{i\omega_m t}$, $E_m^{(-)} = \frac{E_m}{2} e^{-i\omega_m t}$ be the positive and negative wave components of the electric field with the frequency ω_m . Thus the second order of the polarization is

$$\vec{P}^{(2)} = \epsilon_0 \sum_{m,n} \chi^{(2)}(\omega, \omega_m, \omega_n) (E_m^{(+)} + E_m^{(-)}) \cdot (E_n^{(+)} + E_n^{(-)}) \quad (1.2)$$

with the second order dielectric susceptibility $\chi^{(2)}$ depending on the mixed frequencies ω_m, ω_n and the resulting frequency ω .

The different frequency components of the electric field combine to oscillations of the polarization with new frequencies. Considering just two frequency components $m, n = \{1, 2\}$, the polarization contains five newly generated frequency components:

- $P \propto e^{i2\omega_1 t} + c.c.$ is the **second harmonic** of ω_1 as ω is twice ω_1 . This process is called **second harmonic generation (SHG)**.
- Similarly $P \propto e^{i2\omega_2 t} + c.c.$ is the second harmonic of ω_2 .
- $P \propto e^{i(\omega_1+\omega_2)t} + c.c.$ is the **sum frequency generation (SFG)** with the sum $\omega = \omega_1 + \omega_2$.
- $P \propto e^{i(\omega_1-\omega_2)t} + c.c.$ is the **difference frequency generation (DFG)** with the positive difference $\omega = |\omega_1 - \omega_2|$ as frequencies are always positive.

- $P \propto e^{0-it}$ does not oscillate anymore and is called **optical rectification** with $\omega = 0$.

The dielectric polarization is a source of an electric field, therefore those oscillating polarization components are sources of electromagnetic waves with the corresponding frequencies. This series of steps from an oscillating electric field through an oscillating polarization to an electric field oscillating with a different frequency is useful to produce or amplify coherent radiation at wavelengths, where no suitable laser medium exists.

Inserting the dielectric polarization (equation 1.1) up to the second order into the wave equation

$$\nabla \times \nabla \times \vec{E} + \frac{1}{c^2} \frac{\partial^2}{\partial t^2} \vec{E} = -\frac{1}{\epsilon_0 c^2} \frac{\partial^2}{\partial t^2} \vec{P} \quad (1.3)$$

we get two interesting relations

$$\frac{1}{\omega_c} \frac{\partial}{\partial z} I(\omega_c) = -\frac{1}{\omega_a} \frac{\partial}{\partial z} I(\omega_a) = -\frac{1}{\omega_b} \frac{\partial}{\partial z} I(\omega_b) \quad (1.4)$$

$$\frac{\partial}{\partial z} I(\omega_c) + \frac{\partial}{\partial z} I(\omega_a) + \frac{\partial}{\partial z} I(\omega_b) = 0 \quad (1.5)$$

for the intensity I of the participating frequency components $\omega_c = \omega_a + \omega_b$ over the propagation distance z . Those two equations show the energy transfer from the waves with the lower frequencies ω_a, ω_b to the one with the highest frequency ω_c in sum frequency generation and second harmonic generation. It is the other way round in difference frequency generation and the energy is transferred from the wave with the highest frequency ω_c to the other waves with lower frequencies. In all cases the total amount of energy is conserved. The loss or gain of intensity of one components is proportional to the frequency of that component [12].

In difference frequency generation, the wave with the highest frequency ω_c is called **pump**, because it gives energy to the whole process like the pump of a laser. The **signal** with frequency $\omega_b < \omega_c$ receives, together with the byproduct **idler** with the frequency $\omega_a = \omega_c - \omega_b$, the energy transferred by the pump. Amplifying the signal in such an **optical parametric amplifier (OPA)** has the advantage over amplification in a laser medium, that any frequency lower than ω_c can be amplified. Furthermore, amplification occurs only while the pump is present, so switching the pump switches the amplification. And last, excess energy is not deposited in the amplifier but extracted either as pump or idler. In a laser, on contrary, it is deposited as heat in the laser medium.

If the optical parametric amplifier is placed in a cavity for the signal, also called resonator, the external source of the signal can be omitted. Any stray photon with a frequency lower the pump frequency is amplified, but only those matching the cavity are fed back and amplified again. Because of the feedback this system is called an **optical parametric oscillator (OPO)**. It works like a laser, but with an OPA as the active medium. Its main advantage is that any frequency below the pump can be generated. Therefore, it is widely tunable and new frequencies are achievable.

Base Setup

Many different combinations of nonlinear processes are able to produce light at 606 nm. Each one requires a matching pump source. The most simple nonlinear setup, at least in principle, is the second harmonic of an infrared laser at 1212 nm. An OPO offers the possibility to decouple pump and output wavelength. The pump wavelength, however, has to be smaller than the output wavelength. As many pump sources are at 800 nm or 1064 nm, an OPO alone in combination with such a pump is unable to achieve an output at 606 nm.

Based on those pump sources, a combination of OPO with SFG or with SHG is able to output light at 606 nm. Many different combinations are possible in theory and some have been tested by different groups for similar wavelengths. An OPO can generate light at 1212 nm from a pump at 1064 nm and a second step of SHG generates the desired output. However, the OPO's unused output, idler or signal, is at 8700 nm, where it is difficult to find a transparent nonlinear material, in order to let it resonate as signal or extract it as idler [14]. If the pump beam is frequency doubled before the OPO, the unused output's wavelength in above setup is reduced to 948 nm. This setup of a 1064 nm pump source, SHG, OPO, and SHG again is feasible and has been done by Mhibik *et al.* for 602 nm [15].

Nonlinear processes require high intensities for high conversion efficiencies therefore they should take place in a cavity for higher intensities through resonance. Mhibik *et al.* placed the SHG in the OPO's cavity in order to use the high signal intensity in the cavity for the SHG [15]. The first SHG needs another cavity. Even with those cavities, some pump radiation remains unused, because each step requires and consumes only radiation produced by the step before. Moore and Koch propose to combine an OPO with SFG. The sum frequency generated out of the OPO's signal and the pump has a wavelength shorter than the pump wavelength. In this case both processes, OPO and SFG, consume pump power and their combination offers a better conversion efficiency [14].

Lockheed Martin offers the *Aculigh Argos 2400* system as a commercial application of the OPO and SFG combination. Its pump source is an ytterbium doped fiber laser and fiber amplifier (YAR-15K-1064-LP-SF by *IPG Photonics*), which emits light at 1064 nm with up to 15 W output power. The OPO's signal, with a wavelength at 1408 nm, generates together with the pump the sum frequency of 606 nm. We currently use the Argos system, but several attempts to improve its linewidth below 58 kHz by changing the active stabilization failed [5].

We know the complexities of the Argos system better than those of a frequency doubled laser diode, especially as the Argos system was designed in collaboration with our group [7]. Therefore, we decided to follow the same approach in order to create a system either with a smaller linewidth or which grants more insight in order to improve the Argos' linewidth.

We want to use the Argos' fiber amplifier as the pump source for our new laser system. The setup needs, beside this pump source, four elements: The OPO requires a cavity and a nonlinear medium for efficient conversion. The SFG requires a nonlinear medium as well. Finally, a low finesse etalon is used to choose and maintain a single longitudinal signal mode because the cavity and the amplification of the nonlinear medium allow multiple signal wavelengths.

The nonlinear medium for SFG could be placed either inside the cavity or outside. If it is outside, the idler or a part of the signal has to be used, which reduces the signal energy in the OPO's cavity, and the SFG needs its own cavity for higher intensities increasing the setup's complexity. Placing the SFG medium in the OPO's cavity solves both challenges: no energy has to be extracted from the cavity and the signal intensity is already high through the OPO's cavity.

Light beams diverge and intensity decreases, therefore each nonlinear medium has to be in its own focus, or both media have to be combined in a single medium. A combined medium needs two sections, one for the OPO and one for the SFG. In the case of two separate media, the cavity design gets more complicated as the eigenmode has to have two small foci. In the case of a single medium, both sections are closer to the focus than two separate media around a single focus. Aculight follows the approach of a single crystal in their Argos system and so do we. In order to maximize the interaction length, a 50 mm long nonlinear medium was chosen, compatible with the mount of the Argos system already in use.

The following sections describe the cavity, nonlinear medium, and etalon in detail.

1.1.2 Cavity Design

The cavity determines the mode of the signal. On one hand, the curvature of the used mirrors and other optical elements determine how the transverse mode is shaped in the cavity. On the other hand, the frequency dependent loss per round trip determines, together with the amplification of the nonlinear medium and the etalon, which longitudinal mode or modes are present. The goal of this work is a system with a reduced linewidth. Therefore, fewer longitudinal modes are better, for the signal is a critical part of the desired orange output. In the best case just one longitudinal mode is present and does not change over time.

There are two fundamental types of cavities. In a **linear cavity** the light passes the cavity twice per round trip, once in one direction and then in the other direction. The simplest example are two mirrors between which the light is reflected back and forth. There can be more mirrors between them, but those two mirrors reflect the beam into itself. In a **ring cavity** however, the light may propagate only in one direction, for example in a triangle between three mirrors. A ring cavity requires at least one more mirror than a linear cavity, but offers the advantage, that the light might travel in a single direction.

If the OPO's cavity is a ring cavity, the signal propagates only in one direction and the sum frequency is generated only in that same direction, which simplifies the setup and increases the usable output power. Furthermore, Bosenberg *et al.* observed over 220 longitudinal modes in a linear cavity. A ring cavity with the same curved mirrors, same length and the same etalon had only a single longitudinal mode [16]. For those two reasons we chose a ring cavity.

A cavity built only from planar mirrors is barely stable as a tiny misalignment prevents a ray from matching its starting point after one round trip. Curved mirrors allow a stable cavity. Both Bosenberg *et al.* and Aculight use two concave mirrors curved with a radius of 100 mm next to the nonlinear medium and two more planar mirrors for the ring cavity [7, 16]. Those setups are stable cavi-

ties, therefore we use the same mirror configuration depicted schematically in figure 1.1.

The cavity's eigenmode was simulated with a Gaussian beam in order to calculate the distances between the mirrors. For best conversion efficiency the focus should be in the center of the nonlinear medium and the Rayleigh length z_R of all participating beams should be half the medium length. That way all beams behave similarly and the best compromise is reached between focus size and divergence [17]. Those requirements fix the beam parameter inside the nonlinear medium.

Optical elements in the cavity change the beam through reflection on curved mirrors or diffraction. Optical 2×2 matrices can be used to calculate those changes, notwithstanding that they originate from ray optics. A ray can be described by its distance r from the optical axis and its angle r' to the axis. If position and angle are combined in a vector $v = (r, r')^T$, multiplying a 2×2 matrix with the vector gives the output for position and angle depending on both input components. Several matrices can be multiplied in order to describe the change caused by the combination of the respective optical elements, because matrices are linear. Basic matrices are those for propagation, refraction, and reflection. The whole cavity can be described by a combination of those basic matrices.

The complex **beam parameter** $q = z - iz_R$, with the **Rayleigh length** z_R , describes a Gaussian beam's shape at a propagation distance z from the focus. Although the beam parameter's propagation is not a simple product with a matrix, the optical matrix method is still useful, because it can combine the effect of several optical elements into a single matrix. After the elements described by the matrix $\begin{pmatrix} A & B \\ C & D \end{pmatrix}$, the beam parameter is

$$q' = \frac{A \cdot q + B}{C \cdot q + D} \quad (1.6)$$

for a beam parameter q beforehand [12].

After one round trip in the cavity, the eigenmode's beam has to have the same size and curvature, and therefore the same beam parameter. If the matrix of equation 1.6 describes the cavity, q' has to be equal to q and the equation can be solved for q . Conversely the known beam parameter in the focus defines the relationship between the distances between the mirrors.

For a simple setup, the cavity should be symmetrical. Furthermore, a distance of $a = 46$ mm between a curved mirror and the edge of the nonlinear medium was chosen. As a result, the optical path from one curved mirror to the other one via

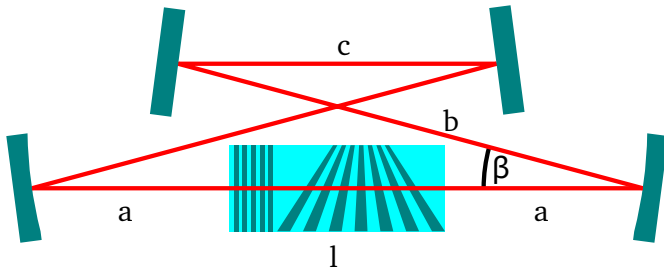


Figure 1.1: Schematics of the ring cavity: Turquoise are the mirrors, red is the beam path and light blue is the nonlinear medium of length l . The bottom mirrors are curved.

the planar ones has to be 300 mm. A bow tie configuration reduces the cavity's size. All those requirements do not define the reflection angle at the mirrors, therefore an angle of 15° between incident and reflected beam was chosen to keep the cavity small and to have some separation between the beam paths. This angle defines the position of the planar mirrors and the whole cavity is defined. Figure 1.1 shows the resulting scheme of the cavity. The eigenmode's beam waist is 71.4 μm.

1.1.3 Nonlinear Crystal Design

Some crystals offer high nonlinear susceptibilities, therefore we want to use one as our nonlinear medium. Unfortunately, the high susceptibility is not enough. The same three frequencies may participate in sum frequency generation or difference frequency generation, only the energy transfer differs. The first process transfers energy to the highest frequency, the latter from the highest frequency. The phase difference between the waves determines which process takes place and its effectiveness. Efficient conversion requires control of the phase difference.

Phase Matching and Quasi Phase Matching

A wave's phase depends on one hand on time and frequency and on the other hand on propagation distance and the wave vector. The wave vector

$$\vec{k} = \frac{2\pi}{\lambda} \vec{e}_z \quad (1.7)$$

indicates the propagation direction with the unit vector \vec{e}_z and is inversely proportional to the wavelength λ .

In the nonlinear processes SFG and DFG, the wave vectors have to be added up or subtracted, respectively, similar to the frequencies. The generated wave, however, propagates with its own wave vector dictated by its frequency. The **phase difference** between the lower frequencies ω_a and ω_b on one side and the highest frequency $\omega_c = \omega_a + \omega_b$ on the other side is

$$\Delta\phi = \phi_a + \phi_b - \phi_c \quad (1.8)$$

with the phases ϕ_a , ϕ_b , and ϕ_c of the corresponding frequencies. Its spatial evolution depends on the **wave vector mismatch**

$$\Delta\vec{k} = \vec{k}_a + \vec{k}_b - \vec{k}_c \quad (1.9)$$

with the respective wave vectors \vec{k}_a , \vec{k}_b , and \vec{k}_c .

The energy transfer between the three waves depends on the phase difference. Without a phase difference, no energy is transferred. If it is $\frac{\pi}{2}$, the lower frequency waves are ahead of the highest frequency wave and amplify the highest frequency through SFG [18]. In all other cases, the combination of the lower frequency waves can be described by the sum of two components, one with a phase difference of $\frac{\pi}{2}$ and one without a phase difference. Only the component projected onto the imaginary axis, with a phase difference of $\frac{\pi}{2}$, participates in

the energy transfer. This component is $\sin(\Delta\phi)$ times the total amplitude and the energy transfer scales with that factor. If the factor is negative, the lower frequencies lag behind the highest frequency and get amplified by DFG.

If the wave vector mismatch does not vanish, the relative phase grows with the propagation distance and the nonlinear process oscillates between DFG and SFG. In consequence, a wave being amplified during one half period is depleted during the other half. The intensity oscillates in that case with a low amplitude and no substantial conversion takes place. The oscillation's half period has the length

$$l_c = \frac{\pi}{|\Delta\vec{k}|} \quad (1.10)$$

and is called **coherence length** [18].

If the refractive indices were the same for all waves, equation 1.9 could be reduced to the sum of the frequencies $\omega_a + \omega_b - \omega_c = 0$ and the phase difference would be constant. In consequence, the amplified wave would grow exponentially, as long as the pump intensity stays approximately constant. Dispersion causes, however, in many cases different refractive indices and a nonzero wave vector mismatch. **Phase matching** describes any method which maintains a constant phase difference in order to achieve an efficient conversion.

Especially for second harmonic generation, it is sometimes possible to achieve equal refractive indices, because just two waves interact. One possibility is that at a certain temperature both refractive indices are the same, for the temperature influences refractive indices. Another possibility, more often used, is **critical phase matching** which uses birefringence. The refractive index of a birefringent material depends on the angle between the light's polarization and the crystal's optical axis. For the same polarization, the refractive indices of both frequencies are probably different. If their polarizations are, however, orthogonal, the refractive indices of both waves can be the same for a certain angle between the polarizations and the crystal's optical axis [12].

Birefringence makes critical phase matching possible but causes also problems reducing conversion efficiency. First, the polarization of the waves in regard to the crystal is determined by the phase matching condition and it is not possible to use the maximum dielectric susceptibility a material offers. Second, the phase matching is tuned by rotating the crystal to the necessary angle, therefore the beams do not always enter at right angles. Birefringence causes different refraction angles, which causes the beams to propagate in different directions and reduces the interaction length and conversion efficiency.

In **quasi phase matching** (QPM) the crystal and the waves' polarization may be oriented for the highest dielectric susceptibility, which can be several times that of critical phase matching. In order to always amplify the same wave, the sign of the nonlinear susceptibility is alternated with a specific period. That **periodic poling** is achieved for example by applying a series of alternating electrodes onto two sides of a crystal and a high voltage between the electrodes on those two sides. The voltage orients ferroelectric domains in the material and thus the sign of the dielectric susceptibilities [12].

Alternatively, growing a crystal layer for layer produces also a periodic poling. With the electrodes however, almost any structure can be created, for example

several different poling periods in the same crystal.

The polarization's sign depends on the dielectric susceptibility. If the latter changes its sign, so do the polarization and the electric field originated from the polarization. A change in sign corresponds to a phase shift of π . If the poling period matches twice the coherence length, the phase shift happens every half period which applies to the phase difference between the waves as well. As a consequence, whenever the phase difference reaches the value of π or 2π , it gets shifted back to zero or π , respectively. The phase difference remains therefore always in the range of zero to π for SFG or in the range of π to 2π for DFG, depending on the initial phase difference. The initial phase difference depends on the initially present waves. If the highest frequency wave is not present, it gets generated by SFG and the phase difference remains in the SFG range. If one of the lower frequencies is not present, it gets generated by DFG and the phase difference remains in the DFG range.

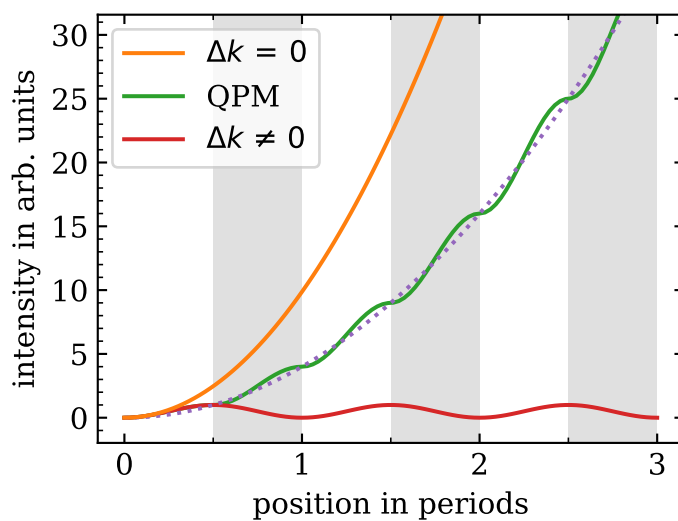


Figure 1.2: Output intensity over propagation distance for nonlinear processes without pump depletion. For critical phase matching ($\Delta k = 0$), the intensity grows exponentially. Without phase matching ($\Delta k \neq 0$), the intensity oscillates with the period $\frac{2\pi}{|\Delta k|}$. If the sign of the nonlinear susceptibility changes with the same period, at the borders between the gray and the white areas, the intensity grows always with the increasing half period of the former oscillation. On average, it grows exponentially as well (the dotted line), but slower than for critical phase matching with equal susceptibility.

The intensity increase depends on the current phase difference $\Delta\phi$ with the factor $\sin(\Delta\phi)$. This factor grows from zero to one and decreases to zero again over half a period after which it is shifted back to the growth phase. Similarly the intensity growth increases and decreases periodically over that half period. As a consequence, the intensity grows on average exponentially, but reduced by the factor $\frac{2}{\pi}$ in comparison to critical phase matching with the same susceptibility. Figure 1.2 shows the intensity over the propagation of several periods in comparison to critical phase matching and no phase matching.

Even though quasi phase matching reduces this **effective nonlinear coupling**

coefficient, the coefficient can still be several times that available to critical phase matching because a higher susceptibility can be chosen by a better orientation of crystal and polarization. For example, the nonlinear material PPLN's highest susceptibility of $25 \frac{\text{pm}}{\text{V}}$ is reduced to effectively $15.9 \frac{\text{pm}}{\text{V}}$ for quasi phase matching, which is still several times larger than the $4.6 \frac{\text{pm}}{\text{V}}$ available to critical phase matching [13].

As the coherence length depends on the refractive indices of the participating waves, so does the poling period. Therefore, a single poling period is the solution for a specific problem. Slightly different frequencies decrease the conversion efficiency. The phase matching can be tuned with the temperature of the crystal, because a change in temperature changes the refractive indices as well. Another possibility is to include several tracks in a single crystal. Each track has its own poling period. If the beam position in the crystal is changed to another track, another poling period is in effect. Similarly, a **fan-out structure** varies the poling period continuously over the crystal position. If the crystal or the beam are moved with respect to each other, the poling period changes continuously as well. Figure 1.1 shows the scheme of a crystal in the cavity, the left part with a constant poling period over the crystal width, the right part with a fan-out structure.

Design of the Crystal

Lithium niobate is a common crystal material for periodically poled nonlinear applications as it offers high susceptibilities [13]. The result is called **periodically poled lithium niobate (PPLN)** which was already used as an example for a nonlinear medium. A magnesium oxide (MgO) doping reduces electron mobility which increases long term stability [7]. We chose such a crystal with a molar doping concentration of 5% magnesium oxide.

We want two processes to take place in the crystal. The first one is the optical parametric oscillation with its difference frequency generation from pump (1063.8 nm) to idler (4351 nm) and signal (1408.08 nm) and with a cavity resonant for the signal. The second one is the sum frequency generation of pump and signal to orange light at 605.982 nm. At 323 K the first process requires a poling period of $27.9 \mu\text{m}$ and the second one a period of $10.44 \mu\text{m}$ [13]. Therefore we need two sections in the crystal, each for one of these processes. The pump and signal have to pass through both sections.

Temperature changes the quasi phase matching through a change of the refractive index and, to a lesser extent, of the crystal length. Both sections are affected at the same time. Similarly, a fan-out structure in each section would couple the phase matching tuning of both sections to each other. As the poling periods are not produced exactly as calculated, they have to be tuned independently in order to match the poling periods to each other. The solution is one section with a fan-out structure and the other one with a fixed poling period. Temperature still modifies both sections, but the fan-out allows to compensate a change in the first section. The temperature dependent signal wavelength change of the SFG section with its shorter poling period is $2.208 \frac{\text{nm}}{\text{K}}$ and therefore larger than that of the OPO section with $0.107 \frac{\text{nm}}{\text{K}}$ in the temperature range of 300 K to 380 K [13]. Consequently, we chose the fan-out for the optical parametric oscillation for tun-

ing and the fixed poling period with temperature tuning for the sum frequency generation.

The longer the current poling period of the fan-out, the longer is the corresponding signal wavelength and the shorter is the idler wavelength. The reduced idler wavelength reduces the phase mismatch more than the increased signal wavelength because of the nonlinear character of dispersion, therefore the wave vector mismatch is reduced and the poling period has to be larger. The same happens with temperature: the higher it is, the higher is the signal wavelength.

In order to calculate the necessary tuning ranges of temperature and fan-out, the worst possible combinations of the different wavelength ranges were simulated: The pump source may change ± 0.7 nm around 1063.8 nm, the signal may be 1405 nm-1411 nm and the output range should be ± 0.5 nm around 605.982 nm. A temperature range of 40°C-60°C is sufficient for the sum frequency generation. That temperature range and the wavelength ranges require a poling period fan-out from 27.76 μm to 28.04 μm for the difference frequency generation.

The lengths of the two sections have to be chosen correctly for maximum overall efficiency, for the OPO section amplifies the signal while the SFG section consumes signal intensity. Amplification and consumption depend on the length of the corresponding crystal section and on the present intensity. If the OPO section is too long, signal intensity is high but the SFG section becomes too short and the SFG cannot take advantage of the high signal intensity. If the SFG section is too long, the SFG consumes too much signal intensity which in turn reduces the OPO efficiency.

We simulated the OPO's signal gain and the signal loss due to SFG, absorption, and transmission at mirrors with the SNLO software for different signal power levels and a pump power of 13 W [13]. If power gain and loss are equal for a given signal power and a given length distribution of the crystal, that power is the maximum for the specific lengths. The highest output power at 606 nm is achieved for a 42.5 mm long OPO section, a 0.5 mm separation for manufacturing, and a 7 mm long SFG section. A simulation with Gaussian beams predicts a visible output of 4.7 W.

For stable simulation results, the SFG section has to precede the OPO section. Whatever the signal intensity is in the beginning, it is led towards some level of equilibrium between gain and loss. If the intensity is above the equilibrium level, the SFG section consumes too much pump and signal intensity such that the OPO cannot amplify the signal in order to replace the consumed amount and the intensity is reduced. For an intensity below that level, the intensity is increased. If the sections were swapped, an intensity above the equilibrium level would cause the OPO to consume too much pump, such that the SFG consumes less signal and the signal intensity increases even further. A too low intensity, on the other hand, would consume more signal, such that it is decreased even more. Although a preceding OPO section doesn't work stable in the simulation, it works in the Argos system [7]. We follow, nevertheless, the simulated approach with a preceding SFG section, which promises more stability [14].

The crystal's manufacturer *HC Photonics* made their own calculations for our wavelength and temperature requirements and delivered a 50 mm long, 12 mm wide, and 1 mm thick lithium niobate crystal, doped with a molar concentration

of 5 % magnesium oxide. The OPO section is 43 mm long and has poling periods from $27.7 \mu\text{m}$ - $28.05 \mu\text{m}$. After a 0.1 mm long separation gap, the SFG section is 6.9 mm long and has a poling period of $10.39 \mu\text{m}$. The crystal's entry and exit surfaces are anti reflection coated for the participating wavelengths. As the manufacturer knows their material better than we do, they got slightly different results for the necessary poling periods compared to our simulation results.

1.1.4 Etalon Design

The cavity's free spectral range of 596 MHz and the amplification bandwidth of the nonlinear crystal of 65.64 GHz permit multiple longitudinal modes for the signal, called **cavity modes**. They may be present concurrently, or the dominant mode may switch over time. In both cases the change of signal frequency changes the orange output frequency as well and increases thus the linewidth. As a countermeasure, we plan to use an etalon in order to enforce a single mode and maintain it over time. The etalon, with its frequency depending transmission, increases the losses for adjacent cavity modes. Because of mode competition, even a small loss can prevent a cavity mode from being present.

On one hand, we want to have a single cavity mode for a small output linewidth, on the other hand we want to be able to switch between two adjacent cavity modes by adjustment of the etalon's transmission center. For the second goal, the etalon linewidth has to be large enough that always at least one cavity mode is amplified while the transmission center transitions from one cavity mode to the next one. At some point both cavity modes might be amplified. The first goal, however, requires such a small etalon linewidth, that only in the case of that transition between two cavity modes, more than one mode is amplified. Additionally, the free spectral range of the etalon has to be larger than the amplification bandwidth, lest multiple etalon modes, of different spectral ranges, may be transmitted fully.

Bosenberg *et al.* and Aculight use low finesse etalons for that application. The former use an etalon of 100 GHz free spectral range and the latter an etalon of 400 GHz [7, 16]. The low finesse, achieved by uncoated fused silica, implies a large etalon linewidth. That may seem to contradict the goal of a single mode, but a reduction of the overall transmission of one cavity round trip, including the etalon, from 99% to 98% reduces the simulated signal power from 100 W to 60 W. Together with mode competition, that power reduction suppresses the modes with reduced transmittance. Figure 1.3 shows the etalon transmission in compar-

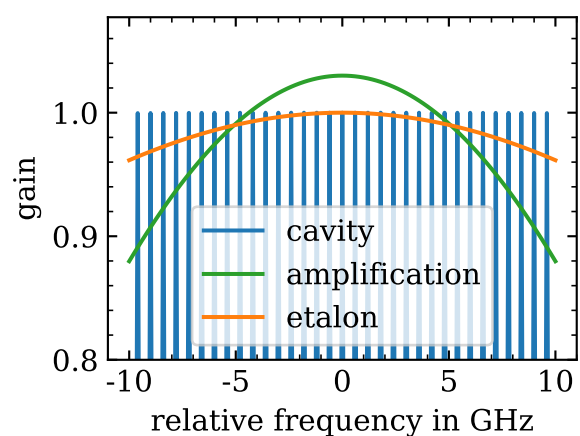


Figure 1.3: Signal gain of the cavity modes, the OPO amplification, and etalon over the frequency detuning from a central frequency.

ison to the cavity modes and OPO amplification.

We chose 100 GHz for the etalon's free spectral range in order to be larger than the amplification bandwidth and smaller than the 400 GHz of Aculight's Argos system whose linewidth we want to improve. A 0.8 mm thick, uncoated YAG plate has a free spectral range of 100 GHz and a finesse of 1, so we use one as our etalon.

The wavelengths transmitted by an etalon depend on the etalon itself and on the angle between the incident light and the etalon's surface normal. The larger that angle, the smaller is the transmitted wavelength. Although the path in the etalon is enlarged, the optical path difference between different reflected or transmitted beams is reduced [19]

We want to choose the current mode and switch between modes by rotating the etalon along an axis orthogonal to the beam. Therefore we attach the etalon to a galvanometer¹ for a high angular resolution and repeatability. The galvanometer has a position sensor and is controlled by an analog PID controller. The controller's signal voltage range is ± 5 V and the galvanometer rotates 1.1° per Volt. A voltage source with millivolt resolution, like our digital analog converters (*National Instruments myDAQ*), gives a resolution of almost 1000 steps per degree. The Argos' etalon resolution is worse with 100 steps per degree.

As the etalon controls the signal frequency, its angular stability is important. In order to investigate the angular stability, a laser beam reflected off the mirror attached to the etalon mount illuminated a screen over 9.5 m away. The spot on the screen did not move visible to the eye. Neither over a few seconds nor for several hours was any movement of the spot on the screen visible. On a beam profiler, the spot center moved less than $10 \mu\text{m}$ in each direction. Therefore, the movement is less than a 10 000th part of a degree. Only in the voltage area of +4 V to +5 V did the spot move. In that range it oscillates with a frequency increasing with voltage. Therefore, the range from -5 V to +4 V is stable and for us usable. The corresponding angular range exceeds the range of the Argos system of $\pm 4^\circ$, of which we normally use little more than one degree.

1.1.5 Pump Injection Setup

For efficient conversion, all beams have to have a Rayleigh length half the crystal length and a focus in the center of the crystal [17]. The most efficient setup shapes signal and visible output, because they are generated in the nonlinear medium. The pump, however, has to be shaped to satisfy that requirement. In our case, the pump source emits its light out of a polarization maintaining fiber coupled with a lens for collimation. That assembly is called **collimator** and includes a ring with a notch in order to orient the fiber and the light's polarization. The light is diverging, therefore, a lens is necessary to focus the beam into the crystal. The curved cavity mirror affects the pump beam like a diverging lens, such that the focusing lens has to counter the mirror as well.

¹It is a galvanometer with a position sensor and a PID controller board made for laser shows with 20 kpps.

Again, optical matrices were used to simulate a Gaussian beam from the collimator to the crystal in order to choose a lens and to position the optical elements right. For determining the beam parameter of the pump leaving the collimator, the beam's radius was measured with a beam camera at different distances from the collimator tip. Fitting the Gaussian beam propagation to these radius measurements returned a beam radius of 0.46 mm and a beam parameter of $(121 - 495i)$ mm at the collimator tip.

Matrices for refraction, with the proper refractive index for 1064 nm and proper curvature, and matrices for propagation modeled the different elements of the setup: the lens, the curved cavity mirror, and the crystal. For a given lens, the matrix equation can be solved to match the beam leaving the collimator to a focus in the crystal with a waist of $62.1 \mu\text{m}$, which is required for the pump in order to have the right Rayleigh length. The solution returns the distance between collimator and lens and the distance between lens and cavity mirror. For a commercially available lens with a focal length of 62.9 mm (*Newport KPX052AR.33*), the entry surface of the lens has to be 110.7 mm from the collimator tip and the exit surface 13.1 mm from the cavity mirror's entry surface. Figure 1.4 shows the beam radius over propagation distance from the collimator to the crystal focus.

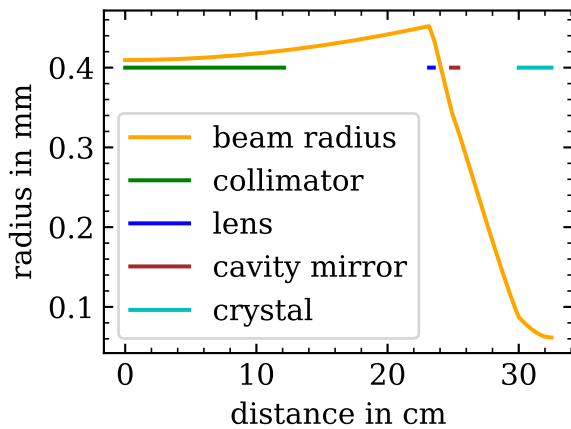


Figure 1.4: Simulation of the pump beam radius from the collimator into the center of the crystal. The colored lines at 0.4 mm radius indicate the position of the optical elements

1.2 Mounting Setup

The optical elements of the laser system need to be mounted somehow. In a first trial they were screwed to the optical table by regular mounts. Later, a custom made mount offered a mechanically more stable system. Finally an acoustic insulation reduced outside perturbations. The following sections explain those three systems in turn and give pointers for adjustment.

1.2.1 Table Mounted Laser System

Initially, the optical elements of pump injection, cavity, and analysis were placed individually onto the optical table as shown in figure 1.5. Between the collimator and focusing lens (L) of the pump injection setup (subsection 1.1.5) are two commercially available mirrors (M1, M2) with a high reflection coating for 1064 nm. They adjust the pump beam's path in order to match the pump to the cavity's eigenmode.

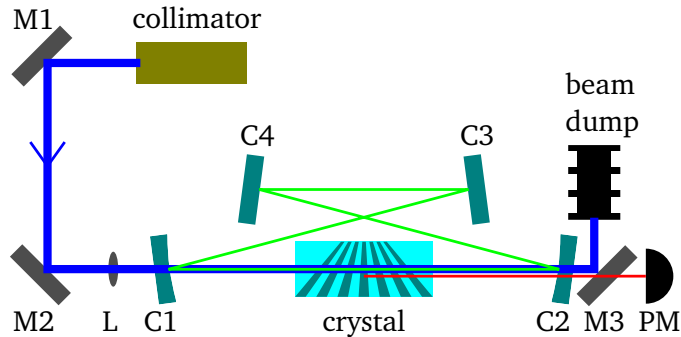


Figure 1.5: Scheme of the free running setup. On top is the collimator emitting the pump (blue). Dark turquoise are the cavity mirrors reflecting the signal (green). In the turquoise crystal they generate the idler (red) which is measured in the power meter to the right. For clarity, the idler is shifted to the bottom. The pump is deposited in a beam dump after the cavity and a dichroic mirror.

The cavity mirrors are 6.35 mm thick calcium fluoride windows, two ones with a curvature of 100 mm (C1, C2) and two planar ones (C3, C4). *Laseroptik* coated them such, that they reflect at least 99.9% of the signal and transmit at least 94.5% of the idler, 98.2% of the pump, and 96% of the orange light. The transmission includes both mirror sides. For improved cavity stability, we chose mirror mounts made out of steel and designed to cause a low distortion (*Thorlabs Polaris-K25F4/M*).

An oven (TC038-D) by *HC Photonics* mounts the nonlinear crystal and offers temperature control by heating. Two translation stages (*Thorlabs XR25P/M*) with micrometer screws adjust the oven's height and lateral position to the beam. A change of height changes the poling period for the current beam path. The lower the crystal in comparison to the beam, the lower is the poling period and the signal wavelength as well. The **crystal position**, as measured by the vertical micrometer screw, indicates how much the crystal has been moved downwards. Therefore the poling period decreases with increasing crystal position.

In order to make the initial adjustment easier, we replaced the **606 crystal**, described in section 1.1.3, with the **OPO crystal**. The OPO crystal has the same outer dimensions and the same material, but a periodic poling fan-out of $27\text{ }\mu\text{m}$ to $30.45\text{ }\mu\text{m}$ and a matching anti reflection coating, which are for DFG only. That way, we were able focus on the

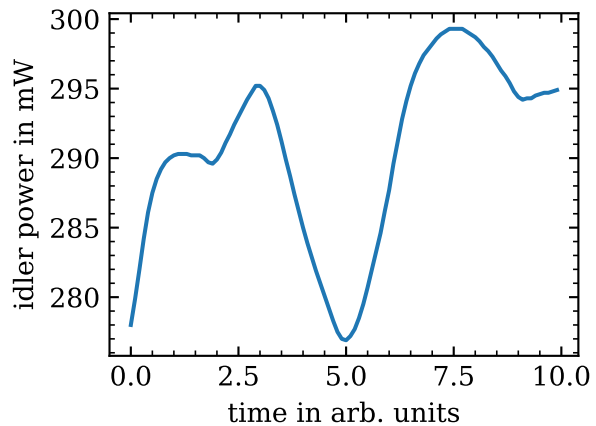


Figure 1.6: Idler output power of the free running setup over the course of a few seconds. A peak to peak variation of 7.7% and standard deviation of 2.2% of the average power of 290.5 mW is clearly visible.

OPO, which uses the DFG, and add the SFG afterwards by swapping the crystals. The output is the idler with a wavelength about 4400 nm.

A dichroic mirror (M3) and a germanium window (not shown) separate the idler from the pump, signal, and visible light. The visible light's origin and use are discussed in the next section. Having isolated the idler, a thermal powermeter (*Ophir 3A, PM*) measures the idler's power. The etalon is not yet installed.

The idler had a power of up to 350 mW at a wavelength of roughly $4.4\text{ }\mu\text{m}$ at a pump power of 9 W. A similar Argos system with a different crystal outputs around 1 W at a wavelength of $3\text{ }\mu\text{m}$. From that, we expect an output power of around 700 mW, because our idler's photons have less energy than one of that Argos system. Our output power, however, was unstable, as figure 1.6 shows. An application of a small force on the mirrors' and crystal's mounts influences the cavity's interference patterns which indicates mechanical instability, for a change in the cavity influences the signal mode. The output power in turn depends on the signal mode and thus an unstable output power is a consequence of a mechanically unstable cavity. The unstable signal mode might be a reason for the reduced output power as a constant mode shift requires an always new buildup of signal power in the cavity.

1.2.2 Adjustment of Optical Elements

Before we continue with the mechanical stability of the cavity, we have to discuss the visible light generated in the OPO crystal. Its poling periods are made for DFG from 1064 nm to 1400 nm and 4400 nm only, nevertheless it emitted green and orange light. Quasi phase matching (see subsection 1.1.3), like any phase matching, facilitates a specific nonlinear process, but it does not prevent other nonlinear processes. They may just be inefficient, because phase matching lacks.

The second harmonic generation of green light at 532 nm from the pump at 1064 nm does not need the cavity for signal resonance. The green light we observed was emitted without a working cavity and its color is similar to light of 532 nm, therefore SHG is very likely. The green light proved invaluable for the adjustment of the cavity, because it is generated parallel to the pump, it is reflected by the mirrors, and it does not require the cavity to work.

The fan-out structure of our crystal requires the beam to propagate at the correct angle with respect to the crystal. At the wrong angle, the poling period would change along the propagation. If the crystal surfaces are at right angles to the ideal beam path, like in our crystal, the green light of the second harmonic can be used for aligning the beam with the crystal. The crystal's surface reflects the green light partially back into the crystal, for the coating's design does not consider

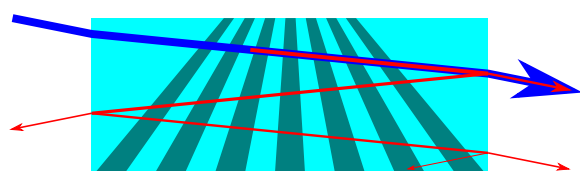


Figure 1.7: Oblique pump beam (blue) in the crystal. The poling period is different along the beam path. The second harmonic (red) is reflected partially at both surfaces. The beams transmitted immediately (top right) and after one round trip (bottom right) are parallel, but at different positions.

that green light. That reflected light is partially reflected at the second surface again. If the beam is at right angles to both surfaces, the first transmitted light and that transmitted after one round trip in the crystal exit the crystal at the same spot. If the angles are not right angles, as shown in figure 1.7, the internally reflected light undergoes a positional change with respect to the immediately transmitted light and leaves the crystal at another spot. Superimposing the green spots on a screen adjusts the second harmonic orthogonal to the surfaces. Most of the time, the SHG intensity reached its maximum, when the spots overlap by adjustment of the pump beam using mirrors M1 and M2. The rest of the time, the overlap was close to the maximum intensity. The second harmonic is generated in the same direction as the pump, therefore adjusting the second harmonic orthogonal to the surfaces adjusts the pump beam as well. In that case of an orthogonal pump beam, the poling period along the beam path is constant. Otherwise the poling period changes along the beam path.

A second use of the green light is the adjustment of the cavity. The cavity's mirrors reflect the green light partially as well, in our case around 80%. The cavity has to be adjusted such, that its eigenmode matches the light generated in the nonlinear medium. By design, the focus sizes already match but the beam angle and position need to be adjusted. The relatively high reflectivity of the mirrors allows the green light to make a whole round trip in the cavity and to be still visible. The transmitted light offers adjustment clues again. This time, the transmitted light has to be observed at two positions of different propagation distance after the cavity. By adjusting two cavity mirrors, the directly transmitted light and the light transmitted after one round trip can be superimposed at both positions thus aligning the cavity to the pump which has been aligned to the crystal beforehand.

Once the cavity is adjusted and the OPO generates the signal, the signal and pump can be combined by SFG to orange light at roughly 606 nm. Without a proper poling period, this process is ineffective, but visible amounts may be generated. We observed light of that color. The SFG requires signal to be present, therefore orange light is an indicator that the OPO works. A change in orange intensity can be perceived much faster by the naked eye, than the idler power by the thermal powermeter. The orange light was, therefore, a good sign when the OPO was active and when probably not.

1.2.3 Cavity Block

The free running setup showed a lack of mechanical stability influencing the signal negatively. In order to have a more stable signal mode, the mirrors and the crystal have to be stable in relation to each other.

A mounting solution consisting of a single piece promises to reduce the relative movement of the optical elements. Therefore, we designed the **cavity block**, a metal block holding all cavity elements. The pump beam's position in the crystal influences the conversion efficiency as well, therefore the collimator and the pump beam's mirror mounts were included, too. The Argos system consists of two parts. One block for the cavity and another one for the pump injection setup. The two part solution allows to access all cavity mirrors from the outside of the

cavity, for example in order to install them. To prohibit a relative movement of the pump injection with respect to the cavity, we chose on contrary a single block containing all elements of both pump injection and cavity.

The fiber amplifier is used elsewhere, too. The collimator's mount has, therefore, to provide such stability, that the collimator can be removed and mounted again without adjusting the cavity. As the collimator is a tube, the collimator mount has a keyhole diameter such, that the collimator rests on the keyhole's edges. Two Screws press the collimator down onto the edges and form the third contact point in the diameter view.

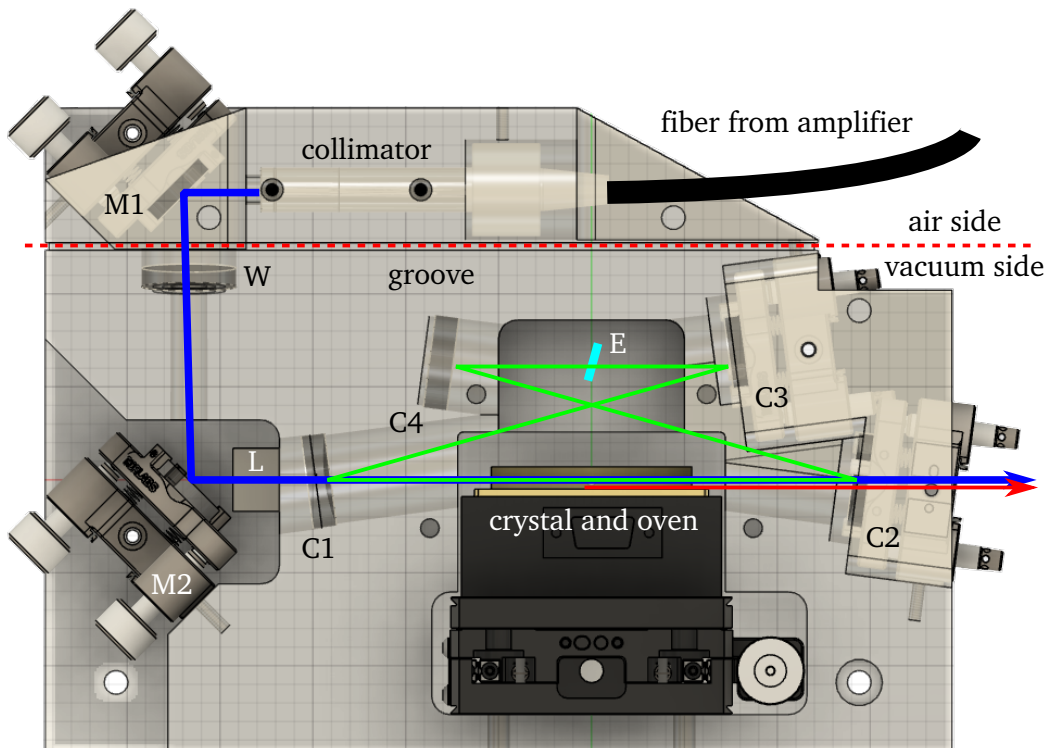


Figure 1.8: Design of the cavity block with the optical elements from subsection 1.2.1 and the position of the Etalon (E), whose mount is not shown. The lens is not visible, only its mount (L). Blue is the pump, green is the signal, and red are idler and orange output together. The red line is shifted to the bottom for clarity. The dotted red line marks the border between air and vacuum sides.

Not all optical elements can be attached rigidly to the cavity block. Two of the four cavity mirrors are needed in order to adjust the cavity and the pump beam mirrors were included for the same reason. Therefore, these four mirrors have to remain adjustable. The other ones can be fixed. The crystal has to be adjustable in height in order to choose a poling period from the fan-out. Finally the etalon has to be mounted such, that it can be rotated.

Commercially available mirror mounts and translation stages offer a better compromise between adjustability and stability than anything we would be able to design and produce ourselves. Therefore, we include those for the adjustable mirrors and the crystal height in our design of the cavity block. They are the products used for the free running setup. Two cavity mirrors are attached directly to

the cavity block, one of which is even glued in. Figure 1.8 shows the scheme of the resulting design of the cavity block and figure 1.9 shows a rendering. The etalon (E) with its galvanometer is attached to the lid of the cavity (shown only in the rendering).

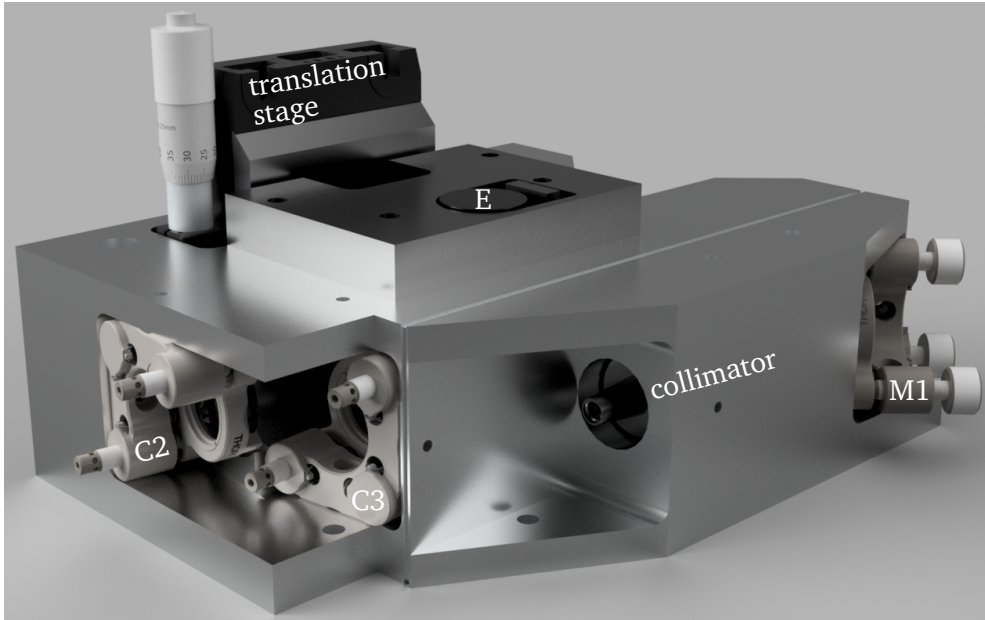


Figure 1.9: Rendering of the cavity block. On top is the translation stage with its micrometer screw. In front of it is the lid with the etalon. Below are visible, from left to right, the cavity mirror mounts, the collimator, and one pump mirror mount.

The goal of this work is the reduction of the linewidth. Sonic waves do have an effect on the optical elements, therefore we want to reduce their influence. Sonic waves cannot propagate in vacuum, therefore we prepared the cavity block for vacuum. As many optical elements as possible should be inside the vacuum, but the fiber has to be attached and the beam has to leave the vacuum chamber.

The fiber housing to the collimator is empty, such that the fiber cannot pass the vacuum border, otherwise air would flow through the fiber housing into the vacuum area. Instead, the vacuum border lies between the pump mirrors M1 and M2. An anti-reflection coated window (W) lets the pump beam enter the vacuum area. In order to prevent any back reflection into the fiber, the window is angled upward at 5°. The distance between the collimator and the lens (L) was revised to compensate the different beam propagation in the 5 mm fused silica window.

Around the cavity block is a groove for an o-ring. Only the collimator and M1 are in air, the rest can be in vacuum, if an external enclosure is designed. Unfortunately, a vacuum enclosure proved to be more difficult to design for the OPO block and no viable solution has been found yet.

In the design process, we simulated the eigenfrequencies of the cavity block and modified our design, in order to increase them and thus make the cavity less susceptible to acoustic perturbations. The eigenfrequencies of the final design are above 8 kHz for a block made of aluminum 7075, which is above common acoustic frequencies. As the acoustic stability of that aluminum alloy is high enough and

it is easier to be milled than harder materials like steel, we chose it for our OPO block.

1.2.4 Acoustic Box

Sonic waves influence the cavity by two mechanisms. First, they imply a pressure and density oscillation in the medium of the cavity. The density oscillations cause an oscillation of the cavity's optical length, because the medium's refractive index depends on the density. The refractive index of air, however, is close to one and the density change is even smaller, such that this effect is negligible. Second, the sonic waves exert forces on the optical elements and cause them to move, such that the geometrical cavity length is changed. To reduce the influence of sonic waves on the signal wavelength, we designed a box for acoustic insulation.

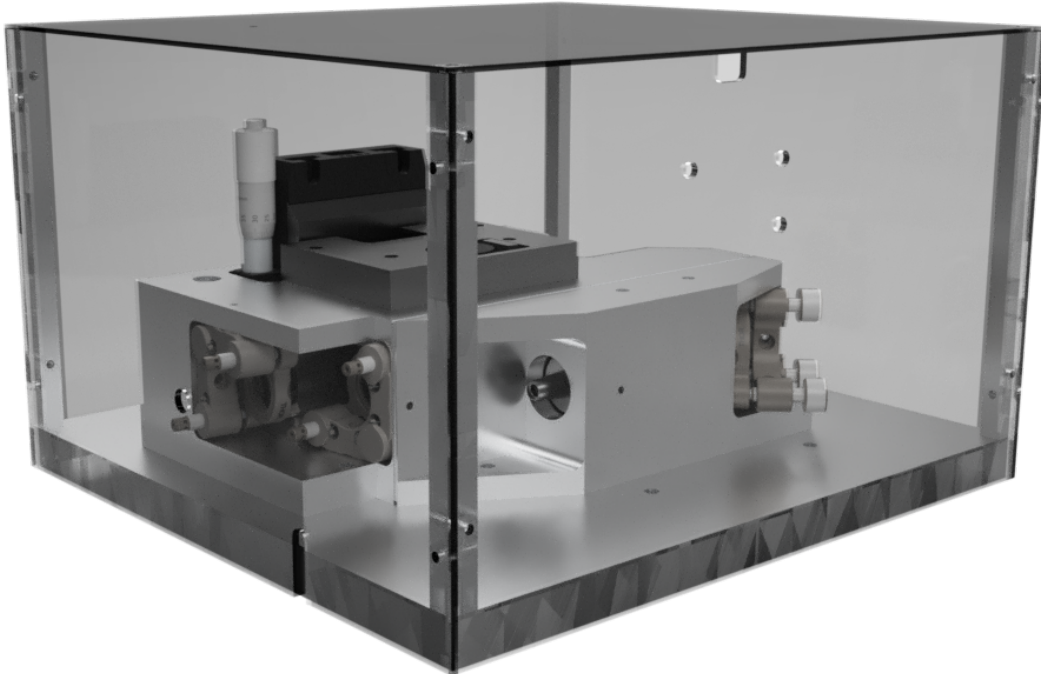


Figure 1.10: Rendering of the acoustic box with the cavity block inside. The side panels and roof are rendered transparent. Wires and acoustic foam are not modeled.

The **acoustic box**, a rendering is shown in figure 1.10, consists of a 10 mm thick aluminum base plate, 1 cm thick square columns and 3 mm thick PVC plates for the sides and top. The PVC plates are lined with a 50 mm thick acoustic absorption foam and contain fitting holes for the fiber from the pump beam, wires for oven and etalon, and for the output of excess pump, idler, and visible light.

Chapter 2

Characterization of the Laser System

Having designed and built the new laser system, we have to characterize it and verify whether it fulfills the requirements of wavelength and power. First the OPO alone is characterized with the OPO crystal for DFG only. Second the crystal is swapped for the 606 crystal and the orange output of the combination of OPO and SFG is characterized.

For the characterization of the laser system, the OPO block is used in order to have a stable mounting of the optical elements. We want to measure the power and wavelength depending on the different parameters of the setup: crystal position, crystal temperature, pump power, and etalon angle.

2.1 Optical Parametric Oscillator Only

First we characterized the optical parametric oscillator alone, using the OPO crystal, which is made just for DFG and outputs light at around 4400 nm. Figure 2.1 depicts the characterization setup for the OPO crystal. A dichroic mirror (DM) reflects the pump into a beam dump and transmits light with a wavelength above 1400 nm, for example the idler. A germanium window (W) reflects and absorbs any visible light and the signal. Only the idler passes both filtering elements.

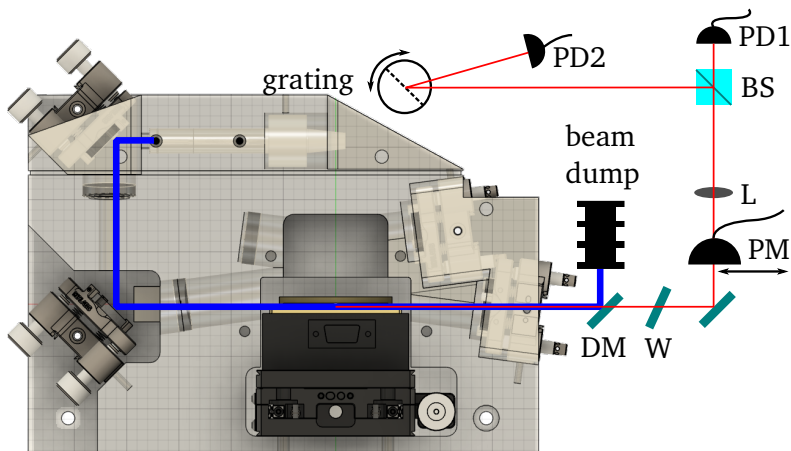


Figure 2.1: Schematic setup for the characterization of the OPO crystal. Blue is the pump, red the idler. The Powermeter is removable. The Spectrometer is depicted only by grating and photodiode.

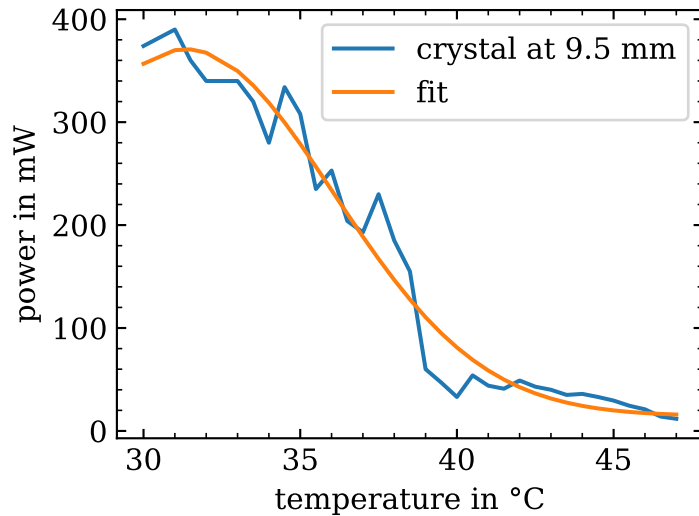


Figure 2.2: Idler power over the temperature of the OPO crystal and a Gaussian fit. Crystal position and etalon angle remained fixed. The wavelength remained at 4144 nm up to 35.5°C and was 4133 nm afterwards. A lower temperature was not possible due to the high room temperature of 25°C.

A thermal powermeter (*Ophir 3A, PM*) measures the idler power. The powermeter is removable in order to measure the wavelength with a spectrometer built by Susanne Otto [20]. A lens (L) provides the necessary collimation. The spectrometer uses a rotating reflection grating with 300 lines per mm. Depending on the current rotation angle, the grating reflects light of a specific wavelength to a photodiode (PD2) susceptible to mid infrared light. The wavelength is calibrated by spectroscopy of gasses. A beam splitter (BS) in front of the spectrometer allows another photodiode (PD1) to measure the power of all frequency components together. That photodiode offers the possibility to observe short term power changes, while the thermal powermeter is slow. The etalon is installed in the OPO block for mode control.

A series of tests characterize different aspects and dependencies of the idler power and wavelength.

Temperature Dependence

First, the output power and wavelength was measured for different temperature settings. The pump power was 12 W, because at that power setting the OPO works well, while the pump laser is not at its maximum output power, which reduces stress. The crystal was at a position of 5 mm. As our oven is not able to cool, the lowest temperature setting was 30°C, for the room temperature was already 25°C and some energy is deposited in the crystal by absorption. That energy heated the crystal and its oven increasing the temperature above the setpoint, while the temperature setpoint was below 33°C. Only from that temperature on did the temperature not rise anymore during a measurement.

The amplification profile is Gaussian for different signal wavelengths. A change in temperature changes the Gaussian's center and thus the distance between the

unaltered signal wavelength and this center. Therefore, the temperature dependence for a constant signal wavelength is expected to be Gaussian as well. Figure 2.2 shows for different crystal temperatures the output power, which declines from its maximum of 390 mW at 31°C to 11.8 mW at 47°C. The form resembles a Gaussian, as expected, but the lower half requires too low temperatures to be measured.

At 35.5°C, the wavelength switched from 4144 nm for lower temperatures to 4133 nm for higher temperatures. At those higher temperatures the power is already too low to be usable, if the crystal position and etalon are not changed. Therefore, temperature tuning of the wavelength is not feasible with the OPO crystal, because the power reduction is too high, before the wavelength changes.

Etalon Angle

Rotating the etalon switched the wavelength basically between the two wavelengths of the previous test, 4133 nm and 4144 nm, while the power remained around 200 mW as shown in figure 2.3. The pump power was 12 W while the crystal remained at a position of 5 mm. The crystal was heated to 35°C to have on one hand high output power and on the other hand prevent the crystal from further heating because of more power being absorbed than dissipated. The erratic movement of the wavelength was not further investigated, as the main project is the generation of orange light with another crystal.

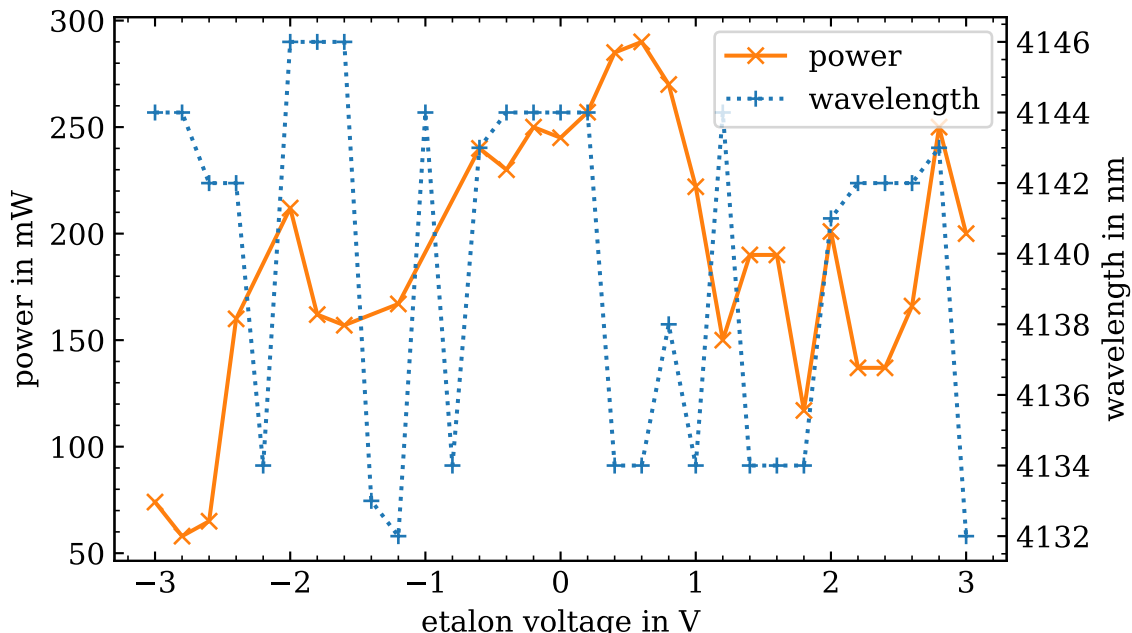


Figure 2.3: Output power and wavelength of the OPO crystal's idler for different etalon control voltages. The pump power was 12 W and the crystal at a position of 5 mm and heated to 35°C.

Pump Power

In a third test, the pump power was varied from 9.3 W to the maximum of 15 W while the crystal remained at 5 mm with a temperature of 35°C.

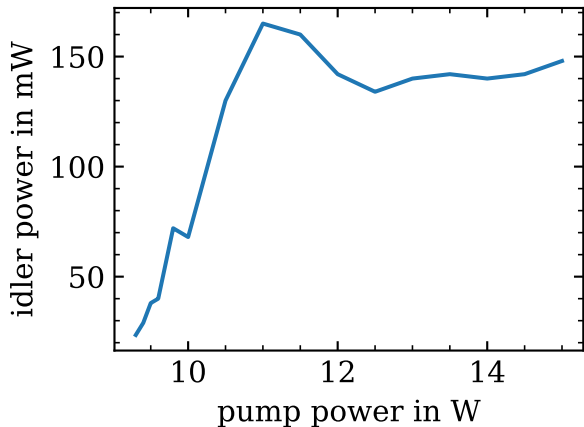


Figure 2.4: Idler power of the OPO crystal for different pump power settings. The temperature was 35°C and the crystal position 5 mm. The etalon angle was not optimized for output power.

increase of output power with increasing pump power.

Figure 2.4 shows the idler's output power over the pump power. For low pump power values, up to 11 W, the output power increases. Afterwards the output power remains at roughly 140 mW. For simplicity, the etalon was not optimized at every power step. Probably another cavity mode would have allowed more output power at higher pump power settings, because 12 W pump power already generated 350 mW idler power in another test. For a complete characterization of this crystal, this test should be repeated, but the power optimized at every step by rotating the etalon. The first part, however, of this test shows the expected increase of output power with increasing pump power.

Crystal position

In a last test, the temperature was held at 35°C, in order to be significantly above room temperature, and the crystal position was changed. The pump power was set to 12 W. Figure 2.5 shows the output power and wavelength for the different positions. This time, the power varied a lot, from under 10 mW to over 140 mW, without a clear structure. We did not optimize the output power for every position by rotating the etalon and changing the temperature. Another etalon angle and another temperature might have led to a better phase matching and higher output power. This lack of optimization is the reason, why the maximum power was less than expected from the temperature dependence measurement shown in figure 2.2.

The wavelength, however, grows clearly linear with the crystal position from 3970 nm to 4500 nm. The crystal was mounted to have its highest poling period for the lowest crystal position. Therefore, the signal wavelength decreases with an increasing position while the idler wavelength increases with an increasing position. The slope of the linear fit is 62.62 nm per millimeter of crystal position. The used micrometer screw promises a wavelength resolution below 1 nm.

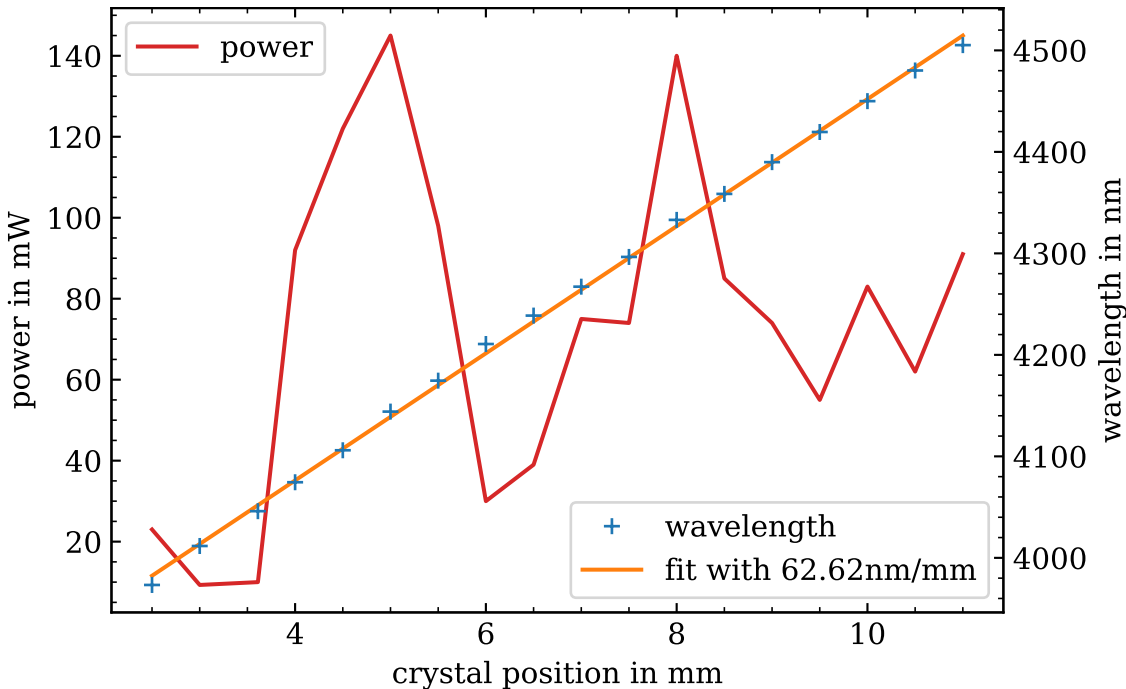


Figure 2.5: Idler power and wavelength over the OPO crystal's position and a line fitted to the wavelength. The temperature was 35°C and pump power 12 W. The wavelength changes 62.62 nm per millimeter crystal position.

Conclusion of the OPO characterization

Those tests show that the crystal position tunes the wavelength most efficiently with a slope of 62.62 nm per millimeter crystal position, while the temperature is useless for wavelength tuning. The temperature, however, is important in order to maximize the output power. The etalon has to be adjusted for the maximum output power as well. The output wavelength is in the range from 3970 nm to 4500 nm.

2.2 Optical Parametric Oscillation and Sum Frequency Generation

Second, we characterize the 606 crystal with sections for DFG and SFG, having exchanged it for the OPO crystal. Its output at 606 nm allows the use of instruments for visible light. The setup is depicted in figure 2.6. Two mirrors (D1, D2), coated by Laseroptik in order to reflect the 606 nm light and transmit the other waves, pump, idler, and signal, separate the orange output from the other beams. The Ophir powermeter (PM) measures the power again and a photodiode (PD) the intensity of the light transmitted by a high reflection mirror (M1) in order to have a short term power resolution. A wavemeter (*High Finesse WS-6*) measures the wavelength of the light, mounted behind a high reflecting mirror (M2) as well.

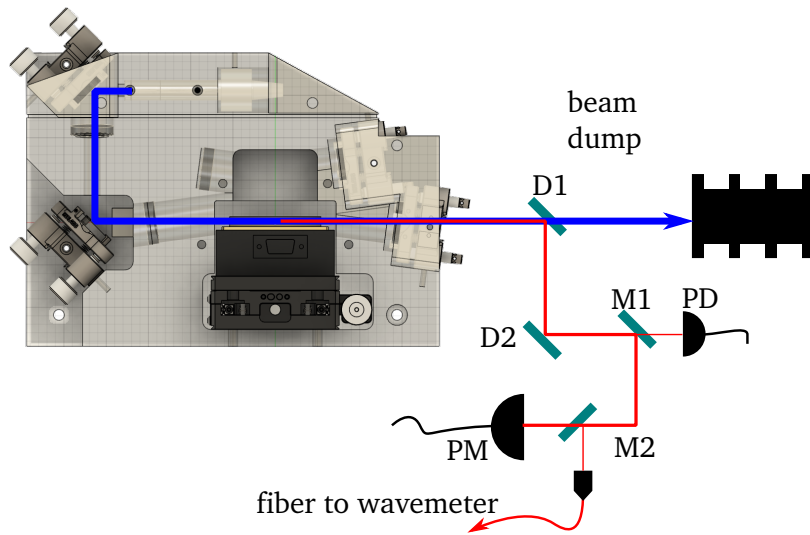


Figure 2.6: Schematic setup for the characterization of the 606 crystal. Blue is the pump, red the orange output. Dichroic mirrors separate the orange light from the rest. A photodiode and the wavemeter measure the light transmitted by high reflective mirrors.

Crystal Position and Temperature

The first experiment with the 606 crystal searched for the best combinations of crystal position and temperature by measuring the orange output power for those combinations. The etalon was not installed, in order to have one parameter less to worry about. The pump power was 12 W.

Figure 2.7 shows the output power over temperature and position. For any temperature setting, there is just a small crystal position range of about 2 mm, where the intensity is above 100 mW. From 37.5°C to 105°C, the maximum is above 1 W. Either a step measured more than 1 W directly, or two measurements lead to expect the maximum between them. When the temperature is increased, the crystal position has to be reduced, which corresponds to an enlarged poling period.

That sharp increase in power, when near the optimal combination of temperature and position, corresponds to the expectation, that only the right combination of both sections' poling periods and temperature allows efficient conversion, because their signal wavelengths match. If the SHG phase matching requires another signal wavelength than that generated by DFG, the process is not efficient. The increased temperature increases the signal wavelength in both sections, but more in the SFG than in the OPO section. Therefore, the OPO section's poling period has to be increased, by decreasing the crystal position, in order to match the increase of signal wavelength, because both, a larger poling period and a higher temperature, increase the signal wavelength in our crystal.

In a second step, the etalon was installed. The power was optimized for different temperatures by rotating the etalon and changing the crystal position. Once the maximum was found, the wavelength was measured. We achieved wavelengths from 605.45 nm to 608.47 nm which includes our desired wavelength of

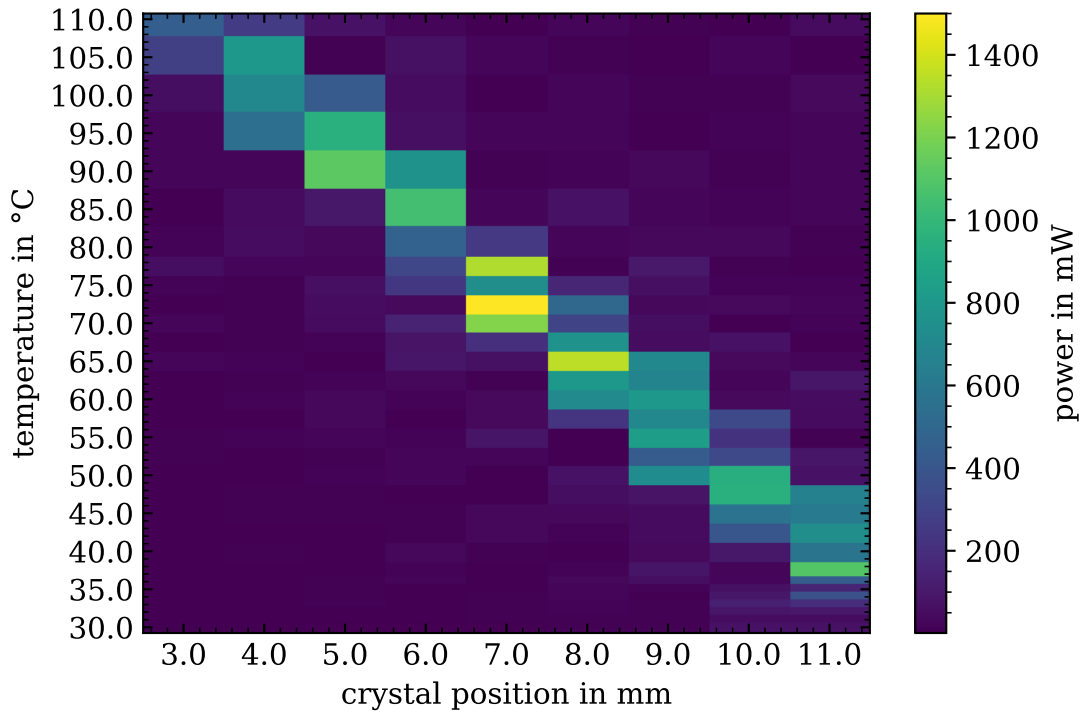


Figure 2.7: Output power of the orange light depending on 606 crystal's position and temperature. The full width at half maximum is just a few steps in each direction. The power maximum is on a straight line. The temperature step size increases with the temperature. The pump power was 12 W.

605.982 nm. Figure 2.8 shows the necessary crystal position and temperature to achieve a certain wavelength with maximum intensity. For one nanometer wavelength increase, the temperature has to be increased by 23.1°C and the crystal position reduced by 2.55 mm. For a wavelength range of 605.5 nm to 607.5 nm, the power was around 1 W, including our desired wavelength. Below that range the power decreases to 0.6 W and above the range down to 0.33 W. Probably, the anti-reflection coatings of mirrors and crystal cause this behavior. An increasing signal power loss per round trip decreases the circulating signal power twice. First the losses itself dissipate power, second the reduced intensity reduces the conversion efficiency of the OPO. The other nonlinear process, the SFG, depends on the signal intensity as well and is reduced, too.

The desired wavelength is already in the achieved range. Nevertheless, the pump wavelength could be reduced in order to reduce the orange output wavelength while the signal wavelength remains the same. That way, the wavelength range of maximum power could be shifted to lower wavelengths and the desired wavelength could be centered in that range.

The new laser system satisfies, according to this test, two of our initial requirements. The wavelength of 605.982 nm is possible with a power of roughly 1 W which is more than the needed 0.5 W.

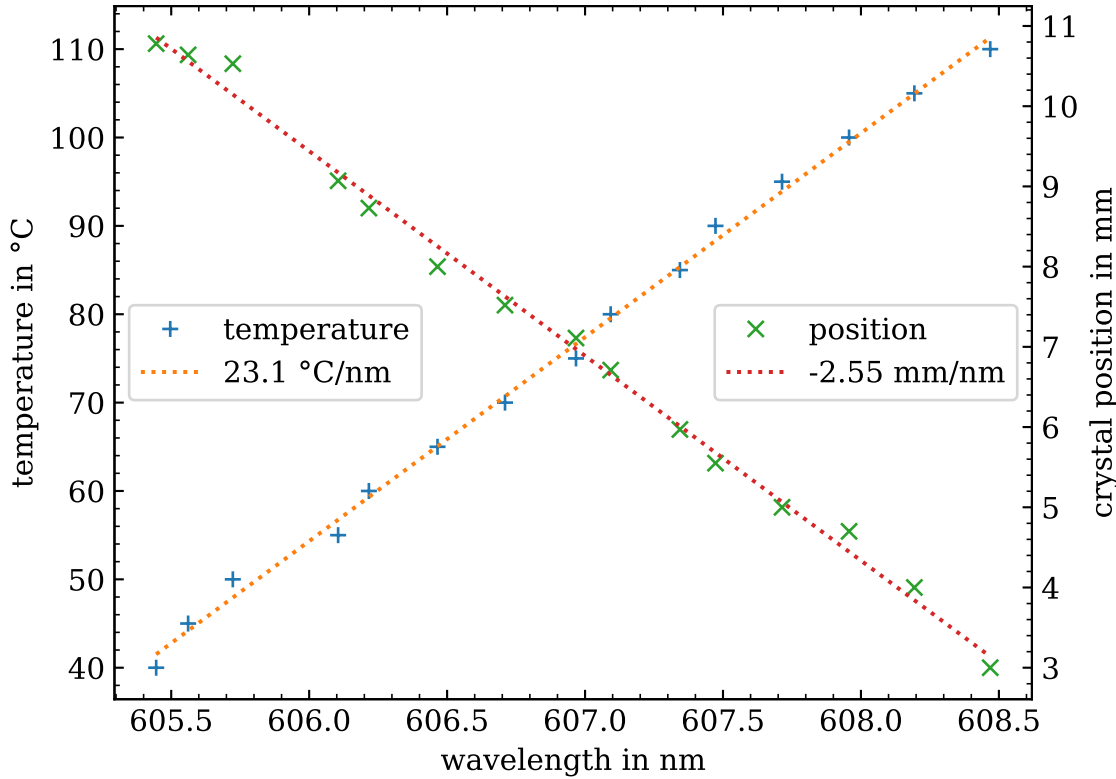


Figure 2.8: Crystal temperature and position for a given wavelength, if the power is maximized by changing the crystal position. Increasing temperature and decreasing position increase the signal wavelength and the output wavelength as well. The pump power was 12 W.

Etalon Angle and Collimator Stability

The last element to characterize is the etalon and its influence on the signal mode and consequently on the orange output. The etalon was rotated by changing its control voltage in steps of 0.1 V, while the pump power remained at 12 W and the crystal remained at a position of 9 mm and a temperature of 51°C. For each step, the wavelength and power of the orange output were measured.

When the etalon rotates towards an orthogonal position to the beam, at roughly 0 V control voltage, the wavelength increases and the power decreases, as shown in figure 2.9. Sometimes, however, the wavelength jumps from a local maximum to a local minimum within one step while the power jumps from a minimum to a maximum. Both, the continuous change and the jumps, are expected. A smaller incidence angle causes a higher transmitted signal wavelength and therefore a higher orange wavelength, too [19]. The wavelength change causes a change in phase matching and therefore in output power as well. The output power does not surpass 1 W anymore, because the etalon increases the losses for the signal which reduces the generation of orange light.

Once the etalon is rotated enough, that the frequency change is equal to the free spectral range of 100 GHz, the system changes to another etalon mode with higher output power and lower wavelength which manifests as a jump of wave-

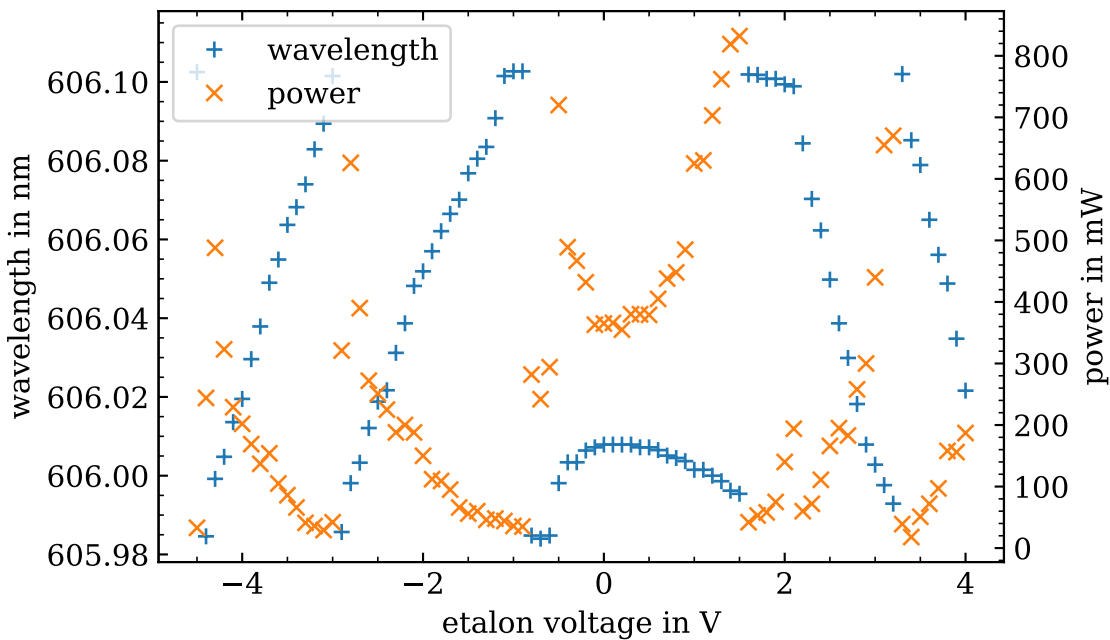


Figure 2.9: Orange output wavelength and power for different etalon control voltages. The wavelength increases towards the orthogonal position up to a mode change, when it starts anew. The pump power was 12 W and the crystal at 9 mm with a temperature of 51°C.

length and power in figure 2.9. The output power starts to oscillate in time at an etalon control voltage of 3.8 V. Additionally, above 4 V the wavemeter measures a rapid oscillation between two wavelengths in accordance to the mechanical oscillation that starts roughly at the same voltage. This result shows the importance of the etalon's stability for the linewidth and that it is stable up to 3.8 V.

The stability and repeatability of the collimator mount has been confirmed as well: the collimator was removed and installed again. The OPO did work regardless, and no negative effect was recognizable. Consequently, the pump source can be used for other experiments as well and switched between the different experiments.

With the etalon we can control the signal mode and thus the orange wavelength and power in fine steps. The etalon, at least up to a control voltage of 3.8 V, and the collimator are mechanically stable for a stable optical output.

Chapter 3

Reduction of Linewidth

After the design and characterization of our laser system, we can turn to our initial goal, the measurement and reduction of its linewidth.

The first section describes the linewidth measurement itself and the second one the setup together with the first results. The third and forth section analyze the influence of sonic waves and the pump source, respectively. In the fifth section an active stabilization is investigated and the sixth one compares the new system with the currently used Argos system.

3.1 Linewidth Measurement

The *Eagle Eye* by *Sirah Lasertechnik* is the core of our linewidth measurements. It consists in a piezo-scannable, confocal, low finesse cavity of a free spectral range of 1.5 GHz and an intensity detector for the transmitted light. As a preparation, a cavity scan returns the detector voltage over the piezo voltage. This scan includes more than one free spectral range and, if the Eagle Eye is illuminated by laser light, two peaks of the cavity's Airy transmission function are visible. Those two peaks allow, together with the known free spectral range, a frequency calibration of the piezo voltage. Furthermore, a fit of the Airy function gives a calibration function for the relationship between detector voltage and frequency deviation, at least for a small range around the peak. In the ready state, the cavity is kept close to the transmission peak by **side-fringe locking**. That technique uses a side slope of the transmission peak, hence the name. It tries to maintain the transmission at half of the maximum intensity, which is at the side slope, by adjusting the piezo voltage. Half the maximum offers not only an approximately linear relationship between intensity and piezo voltage, but offers also directional clues whether the piezo voltage has to be decreased or increased in order to regain the desired intensity. The maximum itself does not offer this information.

During a measurement, the cavity is no longer locked to the half maximum but kept at its current length. The intensity is measured for a specific time period of 60 ms, 100 ms, or 1 s with a constant 15000 data points. The shorter this period is, the higher is the density of data points and the resolvable frequencies. After a measurement, the cavity returns to the locked state and is ready for another measurement. A change in laser frequency implies a change in the transmitted intensity, therefore, the time dependent intensity can be transformed to a time dependent laser frequency with the calibration function. Premise for that measurement is, however, a constant intensity before the cavity. If that intensity

fluctuates, the fluctuation is transmitted onto the detector and interpreted as a frequency fluctuation, even though the frequency had been constant.

The **linewidth** of a laser describes the extension of its spectrum observed during a certain period. One possibility to measure it is the standard deviation of the frequency distribution. That is how the Eagle Eye calculates it from the frequencies measured during the measurement period. It can measure a linewidth as low as 20 kHz, according to the manufacturer [21].

In a series of Eagle Eye measurements under the same circumstances, the results of the individual measurements vary often a lot. Sometimes the standard deviation of the individual results is as large as the average linewidth thus a single measurement is not enough, but a series of measurements has to be taken. Normally we did such a series of measurements, each lasting 100 ms. Figure 3.1a shows such a series of measurements.

The time dependent frequency allows us also to calculate the **power spectral density (PSD)** which describes how the power is distributed among different noise frequency components. From the PSD in turn, the laser linewidth can be calculated. Different noise frequency components contribute differently to the spectral shape of the laser light. The β **separation line**, given by $\beta(f) = \frac{8 \ln(2)f}{\pi^2}$ for a noise frequency f , determines, whether that noise frequency component contributes to the linewidth. If it is below that line, it does not contribute at all to the linewidth, only to the flanks. Otherwise, it contributes with its full value and not only with the difference to the β separation line [22].

3.2 General Setup and First Results

The setup to measure the linewidth is similar to the one used for the OPO characterization, shown in figure 2.6. The YAR-15K fiber amplifier pumps the laser system in the OPO block. Dichroic mirrors separate the orange output from idler and pump. Partially reflective mirrors send most of the orange light to the thermal powermeter, while the wavemeter and Eagle Eye receive a reduced amount transmitted by the mirrors.

Our Eagle Eye is the fiber coupled version. The wavelength meter is fiber coupled as well, therefore a single fiber coupler offers the possibility to change easily between those two instruments. As the Eagle Eye requires more power than the wavemeter, partially reflective mirrors, with a reflectivity of 90%, were used instead of the high reflective mirrors from before.

The average linewidth was 968 kHz in a first series of 1924 measurements, shown in figure 3.1, with a standard deviation of 898 kHz. As that linewidth is larger than our goal, we have to search for the major influence in order to reduce the linewidth.

One possible reason might be, that several cavity modes are amplified simultaneously or that the currently amplified cavity mode changes frequently between different modes. The spectrum of that multimode operation would consist of several peaks. We analyzed the spectrum with a scanning Fabry-Perot cavity (*Thorlabs SA200*) whose free spectral range is 1.5 GHz. A scan over more than one free spectral range showed just two small peaks, separated by the free spectral range,

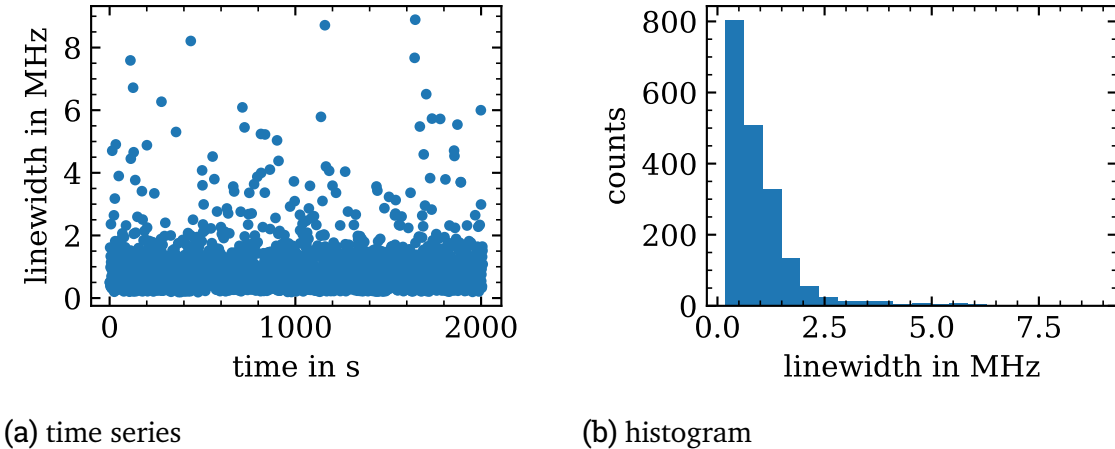


Figure 3.1: First series of linewidth measurements with the 606 crystal. Subfigure (a) shows the linewidth over time and (b) the corresponding histogram. The average linewidth is 968 kHz with a standard deviation of 898 kHz.

which implies, that only one cavity mode is amplified at a time.

In the next sections, we analyze different parts of the setup in order to find the source of the large linewidth.

3.3 Linewidth of Seed and Amplifier

The orange light is the product of the sum frequency generation from pump and OPO signal. The linewidths of those constituents influence consequently the orange linewidth. The propagation of the linewidth in a nonlinear process can be calculated by considering the participating frequencies as instantaneous frequencies varying in time. Let $\omega_a + \omega_b = \omega_c$ be the central frequencies of a nonlinear process and $\delta_a(t)$, $\delta_b(t)$, and $\delta_c(t)$ the deviation of the instantaneous frequency from the respective central frequency. With energy conservation (see equation 1.4), the instantaneous frequencies have to fulfill $\omega_a + \delta_a(t) + \omega_b + \delta_b(t) = \omega_c + \delta_c(t)$. Therefore

$$\delta_a(t) + \delta_b(t) = \delta_c(t) \quad (3.1)$$

is the relationship between the different frequency deviations. If one deviation is zero, for example $\delta_b(t) = 0$, then the other deviation $\delta_a(t)$ equals the right side $\delta_c(t)$ [23].

In our case, the pump deviation is distributed between signal and idler in the OPO. The cavity determines the signal deviation, while the idler deviation depends on the signal deviation and pump deviation. In the SFG the orange light's deviation is the sum of the signal's and the pump's deviation. Consequently, the orange light's deviation is at least of the same order of magnitude as the pump deviation. The linewidth depends on the deviation, therefore the orange linewidth is at least similar to the pump linewidth, if no other disturbance introduces additional noise.

We were not able to measure the fiber amplifier's linewidth directly, because the minimum output power is too high for the Eagle Eye. We measured instead

the linewidth of the green second harmonic generated in the nonlinear crystal. At 103 single measurements with the Eagle Eye, the linewidth was on average 414 kHz with a standard deviation of 219 kHz. According to equation 3.1 the SHG's deviation and linewidth is twice that of the pump ones. Even then, the amplifier linewidth with 207 kHz is a considerable part of the orange linewidth.

The YAR-15K amplifier has an integrated seed fiber laser, but their fibers are coupled externally which allows us to use an external seed laser. In order to reduce the pump linewidth, we used another ytterbium doped fiber laser (*Koheras Adjustik Y10 PM PztM* by *NKT*) with a smaller linewidth as a seed laser for the fiber amplifier. In order to measure that linewidth, the Adjustik seed laser's fiber was coupled directly to the Eagle Eye. A series of more than 500 individual measurements resulted in an average linewidth of 32 kHz with a standard deviation of 9 kHz. The SHG of the combination of Adjustik seed laser and YAR-15K amplifier has a linewidth of 107 kHz with a standard deviation of 6 kHz in 221 single measurements.

The Adjustik seed laser does not only reduce the SHG linewidth from 419 kHz to 107 kHz, but causes also a greatly reduced variation for the standard deviation from more than half the average to less than 3% of the average linewidth. Even with the worse seed laser, the pump linewidth of 207 kHz is a large, but not the main part of the orange linewidth of 1 MHz.

3.4 Influence of Sonic Waves

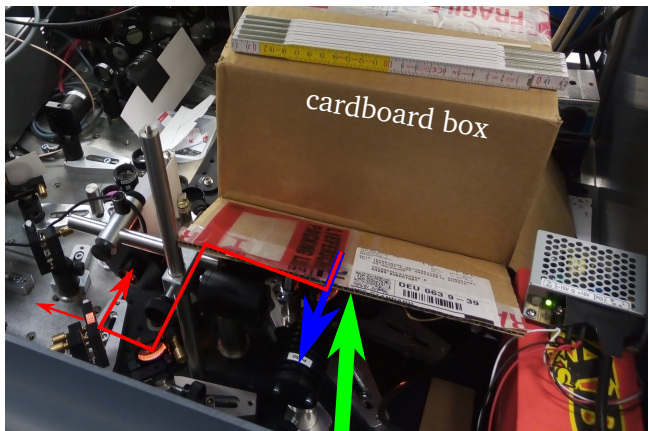


Figure 3.2: Setup with the cardboard box around the cavity block. The pump (blue) leaves the box into the beam dump and the orange light (red) to the power meter. A small amount is transmitted by a mirror to the Eagle Eye. The sonic waves' direction in the box is green.

Eye still measured the orange linewidth with the same setup from section 3.2.

In a first test series, the influence of short events were investigated. Timing a perturbation with an Eagle Eye measurement is not possible. Instead, the Eagle

If the pump does not form the main part of the orange linewidth, the signal has to be the major factor and the signal wavelength depends on the cavity. Sonic waves and mechanical oscillations in the setup have a major influence on the signal wavelength and consequently on signal linewidth which transfers to the orange linewidth. Therefore, we tested how acoustic insulation and excitation influence the linewidth. It is difficult to measure the signal wavelength and we want to know the influence on the whole system, therefore, the Eagle

Eye was again exchanged for the scanning Fabry-Perot-Cavity which we scanned with a repetition rate of 50 Hz. The control module outputs a trigger signal at the beginning of each ramp of the piezo control voltage. With that trigger signal and with the high repetition rate, we were able to monitor the change of the wavelength with an oscilloscope in real time. Loud clapping in the hands or tapping the cavity block or the mounts of the pump adjustment mirrors did not affect the position of the transmission peak. Heavy taps on the cavity mirror mounts, however, or light taps on the adjustment screws of those mirror mounts made that transmission peak move. A gust of wind, made by moving a large Plexiglas panel, affected the wavelength as well. Those tests show the negative influence of mechanical movement and call for some protection.

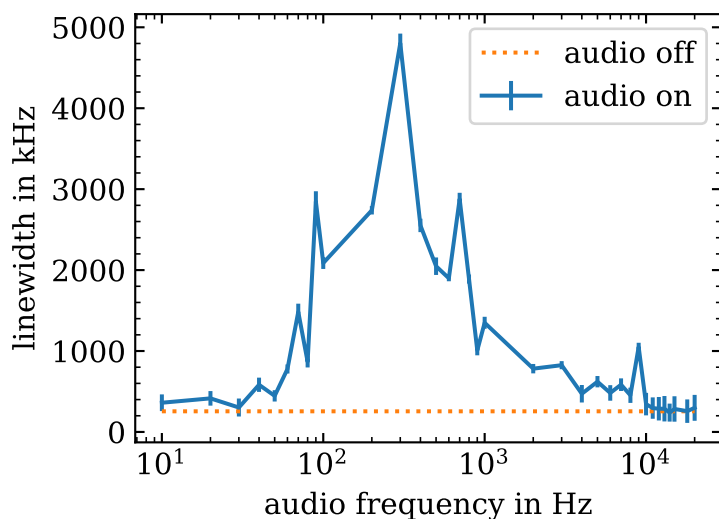


Figure 3.3: Average laser linewidth over the audio frequency at which the system was perturbed. The frequency scale is logarithmic. The errorbars show the standard deviation of the linewidth. The orange, dotted line is the reference of 255 kHz, the linewidth without any audio perturbation.

A simple box made out of cardboard was put on top of the cavity block as shown in figure 3.2. It shields the cavity block and its optical elements a little bit, but leaves large holes, because it was not custom made with matching holes for cables, fiber, and the output beams. Despite this bad insulation, the linewidth is reduced to 348 kHz with a standard deviation of 185 kHz in 304 measurements of the Eagle Eye. Here the internal seed laser was used. With the Adjustik seed laser, the linewidth is further reduced to 263 kHz with a standard deviation of 159 kHz in 525 measurements. The Adjustik seed laser is used for all following experiments.

The previous experiment proved the importance of acoustic insulation. In order to find out which acoustic frequency influences the laser system the most, a large loudspeaker was placed in front of the cavity block, oriented towards the exit side. The speaker was, where the photographer stood in figure 3.2. On that side the cardboard box has a large opening, where the sonic waves could enter.

For different frequencies, the loadspeaker was driven with a sinusoidal signal of that frequency and as loud as possible. The frequency was changed in small

steps and after every change, a handful of Eagle Eye measurements were taken. At larger intervals, a series of roughly 60 measurements were taken, in order to have reliable data. The average linewidth of these more ample series are shown in figure 3.3 in relation to the audio frequency. The errorbars represent the standard deviation of the series. With the loudspeaker turned off, the linewidth was on average 255 kHz. The remarkably low standard deviation, in comparison to the one of section 3.2, which was almost as large as the average itself, shows, that even the large linewidths were measured constantly within a small range.

The smaller series give at least a general idea, how the linewidth behaves between two data points of figure 3.3. They showed, that the linewidth does not change monotonously between two measurements, but, that there are large jumps. Between the audio frequencies of 2 kHz and 3 kHz, for example, we measured linewidths anywhere between 500 kHz and 1.5 MHz. Nevertheless, they confirm the reading of figure 3.3, that frequencies between 100 Hz and 1 kHz have the largest impact on the linewidth and frequencies below 50 Hz or above 10 kHz have almost no influence.

In order to reduce the influence of sonic waves further, the acoustic box was placed around the OPO cavity. This gave an average linewidth of 83 kHz with a standard deviation of 44 kHz in 217 measurements. The whole optical table is surrounded by a flowbox: plexiglas plates around the table and a fan on top, which blows filtered air onto the optical table in order to prevent dust from settling onto the optical elements. If that fan is switched off, the linewidth is reduced to 35 kHz with a standard deviation of 10 kHz in 70 measurements.

These tests show, that acoustic insulation is useful in order to achieve a smaller linewidth. The acoustic box did shield the system from sonic waves in air, but did not do so from sonic waves transmitted by the optical table. A flexible mounting solution between the optical table and the acoustic box could provide that. A vacuum enclosure might provide even better insulation insofar no sonic wave can transverse vacuum. Besides those passive solutions, active noise canceling could reduce the sonic waves influencing the linewidth.

3.5 Linewidth of the Stabilized Laser System

Until now, the laser system was left to itself and not actively stabilized. Active stabilization schemes can reduce the linewidth, because they react to a small change of the wavelength with a change in the laser system, in order to maintain a specified wavelength. A stabilization system consists, therefore, of three parts: one part detects a wavelength change, another part influences the wavelength, and the last part, a controller, determines how to change the wavelength influencing part depending on the detected wavelength change in order to reach a desired wavelength.

The following subsections deal with the wavelength measurement part, the whole stabilization setup, and the experimental results.

3.5.1 Pound-Drever-Hall Stabilization

An active stabilization can use absolute or relative wavelength measurements. Comparing the wavelength to that of an atomic transition is an example of the first type. An absolute measurement is especially useful if atomic transitions have to be driven.

The transitions of the praseodymium ions in the Pr:YSO crystal, however, are inhomogeneously broadened, because the praseodymium ions experience different local magnetic fields depending on their neighborhood in the crystal. The different magnetic fields in turn cause different Zeeman shifts such that the transition frequencies are different as well. Taking all ions together, the linewidth of the relevant transition is broadened to several GHz [24]. As any frequency in that range may excite an ion, it is more important that the frequency does not change in time than that it has some specific value.

Cavities offer the possibility of a relative wavelength measurement, because the transmission depends on the distance between the laser frequency and the closest cavity mode. The exact frequency of that mode cannot be determined with the cavity alone, but the wavemeter gives us this information. Cavities as wavelength references work in any wavelength range, not only for certain atomic transitions.

A simple stabilization setup is side-fringe-locking, which tries to maintain the light at the side slope of the cavity transmission. The same information of intensity change that allows the Eagle Eye to match the cavity transmission to the light frequency (see section 3.1) can be used to match the light frequency to the cavity transmission. The major flaw of this scheme is, that a changed laser intensity results in a changed transmitted intensity as well. As a consequence, the stabilization setup tries to compensate the intensity change with a wavelength change, even though the wavelength was right. While the Eagle Eye just has to stay near the transmission peak, the frequency stabilization has to keep a constant frequency and this intensity dependence counteracts that.

An intensity independent stabilization technique, that can be used with cavities, is the **Pound-Drever-Hall (PDH)** laser frequency stabilization. It uses light reflected at the cavity. The light is reflected immediately and does not require the buildup of a standing wave inside the cavity like the transmitted light does. Additionally, the phase shift between the incident beam and the reflected light depends on the difference between the light frequency and the closest cavity's resonance frequency, including the sign of that difference. Far off resonance, the phase shift is π . Therefore, the phase contains information about the needed direction and magnitude of a frequency change in order to match the light frequency to the cavity frequency [25].

The PDH stabilization uses another frequency component to make that phase shift measurable. An electro-optic modulator modulates the refractive index of its Pockels cell with some frequency Ω . The oscillating refractive index adds an oscillating phase term to the light which corresponds to two new frequency components. They have the frequencies $\omega \pm \Omega$ for the original light frequency ω . Those three frequencies, the original one and its two sidebands, are reflected at the cavity and interfere with a beating on a fast photodiode. The beating's phase

depends on the phase difference between the three waves. If the sidebands are far off resonance by a suitable choice of Ω , the beating's phase is the phase shift between incident and reflected beam. A mixer, which multiplies the photodiode signal with the oscillation signal for the electro-optic modulator, and a low-pass filter generate an error signal. That error signal vanishes when light and cavity frequencies match and has an approximately linear slope around that point. It is, therefore, a good foundation for a control loop in order to stabilize the frequency between cavity and light [25].

3.5.2 Stabilization Setup

The stabilization setup is the same we currently use for the Argos system. Its first part, which detects wavelength changes, is based on the PDH stabilization scheme. Figure 3.4 shows the optical elements of that part. A fiber coupler behind one of the partial reflective mirrors transports the orange light from the OPO to an electro-optic modulator (EOM) which is driven at a frequency of 6.25 MHz. Afterwards a polarization maintaining fiber (PM fiber) transports the light to the PDH cavity. A polarizing beam splitting cube (PBSC) and a quarter wave plate ($\lambda/4$) separate the incident beam from the light reflected at the cavity. The beam splitting cube polarizes the light horizontally and the quarter wave plate turns that polarization into a circular polarization. Once the light is reflected, it passes the quarter wave plate a second time and its polarization is again linear, but this time vertically such that it gets reflected at right angles in the beam splitting cube. This reflection hits a photodiode (PD) which measures the power. A lens (L) matches the light beam to the spatial cavity mode.

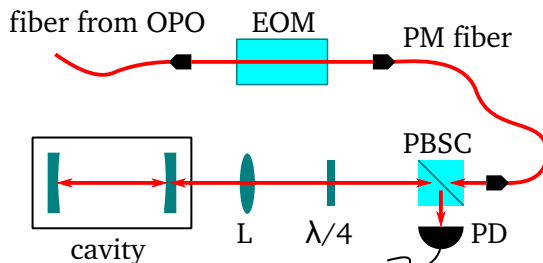


Figure 3.4: PDH stabilization setup for our new laser system. A fiber delivers the light to an electro-optic modulator. Another fiber transports the light afterwards to the cavity which is in vacuum and consists of two curved mirrors. A polarizing beam splitting cube and a quarter wave plate separate the incident beam from the beam reflected at the cavity which is reflected onto a photodiode.

The cavity consists of two concave mirrors with a curvature radius of 1000 mm and a high reflection coating for 606 nm on the curved side. They are connected by a 145 mm long spacer made of ultra low expansion glass. A copper box with Peltier elements maintains a certain temperature, at which the thermal expansion coefficient of the spacer vanishes in the first order. That whole assembly is inside a vacuum box with a pressure of roughly $1 \mu\text{bar}$ in order to reduce the influence of sonic waves and air pressure fluctuations inside the cavity. The cavity length

and mirror reflectivity lead to a free spectral range of 1033 MHz and a linewidth of 330 kHz which corresponds to a finesse of 3140 [7].

The second part of the stabilization, which influences the wavelength, is the Adjustik seed laser, because the seed wavelength becomes the pump wavelength which in turn determines the orange output wavelength together with the OPO's signal. The Adjustik seed laser's wavelength is controlled by two mechanisms. One uses the temperature, because the temperature influences the fiber itself and the fiber length, as its mount expands under temperature increase. That wavelength change is obviously slow as it depends on a temperature change. The wavelength tuning range with the temperature is 1063.62 nm to 1064.12 nm. This mechanism is called **wavelength setting** and is accessed via commands sent over USB.

The other mechanism, the **wavelength tuning**, uses a piezo actuator in order to modulate the wavelength in a small range of 10 GHz, or 1 GHz in fine mode. The manufacturer does not state how this mechanism works. He states, that it can be used reliably for stabilization up to a bandwidth of 20 kHz. The modulation range decreases with the used bandwidth. At 1 kHz bandwidth, for the fine mode which we use normally, the range is decreased to one half and at 10 kHz to a mere 10% [26]. The piezo controlled wavelength tuning is proportional to a differential signal input. An additional factor adjustable between 1 and 0.06 can reduce the tuning range further.

Those two stabilization elements are connected by the third part, a controller. We use the *DigiLock 110* by *Toptica Photonics*. It generates the oscillation signal for the EOM and mixes it with the photodiode signal in order to calculate the error signal according to the PDH stabilization. From the error signal it calculates with a PID (proportional, integral, and derivative) controller a correction signal in order to modify the wavelength. An external circuit converts that signal to a differential one which feeds the Adjustik's wavelength tuning input. If the correction signal comes close to the limits of the piezo's signal range, a computer program changes the Adjustik's wavelength setting in order to keep the piezo signal inside its limits. That is especially needed, because we use the finer piezo range of 1 GHz together with a proportionality factor of 0.1 in order to decrease the frequency range addressed by the DigiLock's correction signal and thus increase the frequency resolution. The combination of both methods ensures on one hand a high precision stabilization and on the other hand a stabilization range larger than the 100 MHz given by the fine mode with a reduction factor of 0.1.

3.5.3 Linewidth with the Active Stabilization

The experimental setup for measuring the actively stabilized linewidth consists of the light generation setup and the stabilization setup. The latter is described in the previous section. The first is the OPO cavity in the acoustic box and the already known series of mirrors. Two mirrors separate the orange light from other wavelengths and other mirrors distribute the power among several instruments. One part is led by a fiber towards the PDH setup in order to generate a stabilization signal and stabilize the wavelength. Light transmitted by another mirror is led towards the wavemeter or Eagle Eye in order to measure the wavelength or

linewidth, respectively.

The linewidth of the stabilized laser system was 25 kHz with a standard deviation of 5 kHz for a closed acoustic box, closed flowbox, and switched off flowbox fan. With an open acoustic box and open flowbox, the linewidth was 26 kHz with a standard deviation of 8.4 kHz, which is barely worse. In fact, another measurement with the boxes closed had a linewidth of 33.6 kHz with a standard deviation of 11.1 kHz. With the same setup at the same day, but without stabilization, the difference between both boxes opened and closed is clearly visible. In the first case the linewidth was 112 kHz with a standard deviation of 77.3 kHz and in the second one it was 59.2 kHz with a standard deviation of 16.6 kHz.

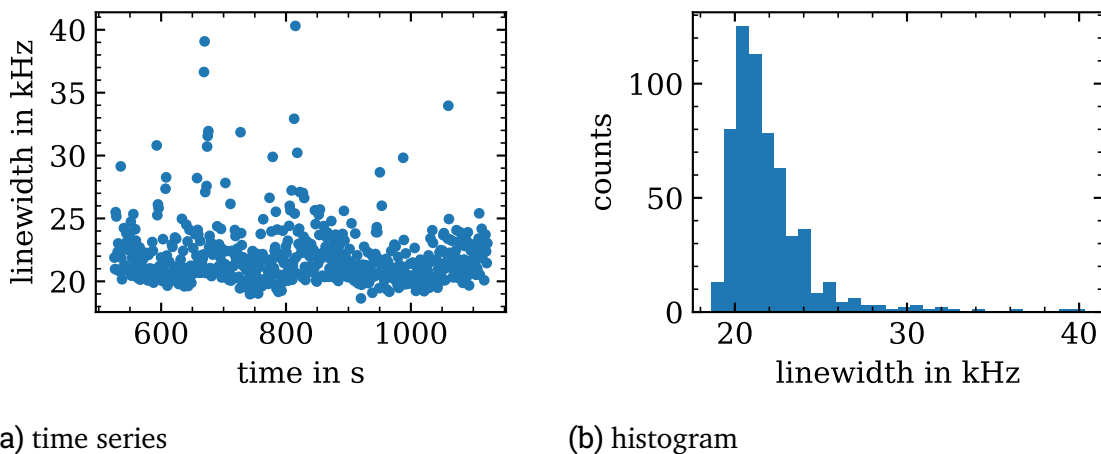


Figure 3.5: Series of linewidth measurements with optimized PID values. Subfigure (a) shows the linewidth over time and (b) the corresponding histogram. The average linewidth is 21.9 kHz with a standard deviation of 2.5 kHz.

The effect of a stabilization system depends on all of its three parts. The wavelength measurement and wavelength control are fixed and cannot be adjusted. The controller, in our case the DigiLock, however, is adjustable, especially the values of the PID controller. By adjusting those parameters, we tried to improve the reaction of the system and reduce the linewidth. Finally we reached a linewidth of 21.9 kHz with a standard deviation of 2.5 kHz in 592 measurements. Figure 3.5 shows the linewidth over time and the corresponding histogram, which are similar to those of the new system's first results shown in figure 3.1, but almost two orders of magnitude better. The linewidths of some single measurements are already at the Eagle Eye's detection limit of 20 kHz, such that the real linewidth might even be better.

The power spectral density gives clues regarding the causes of the linewidth. Figure 3.6 shows the PSD of the pump source, of the orange output without stabilization, and of the orange output with active stabilization. Each one is calculated from measurements lasting 60 ms. The pump's PSD was not measured directly. Instead we measured the PSD of the pump's SHG and divided it by two, for the SHG's PSD is twice that of the pump, similar to the linewidth.

In a range from 100 Hz to 3 kHz, the unstabilized output has a higher PSD than the pump, otherwise the pump is above the orange light. Probably, the system does not react fast enough to incorporate the whole pump noise above

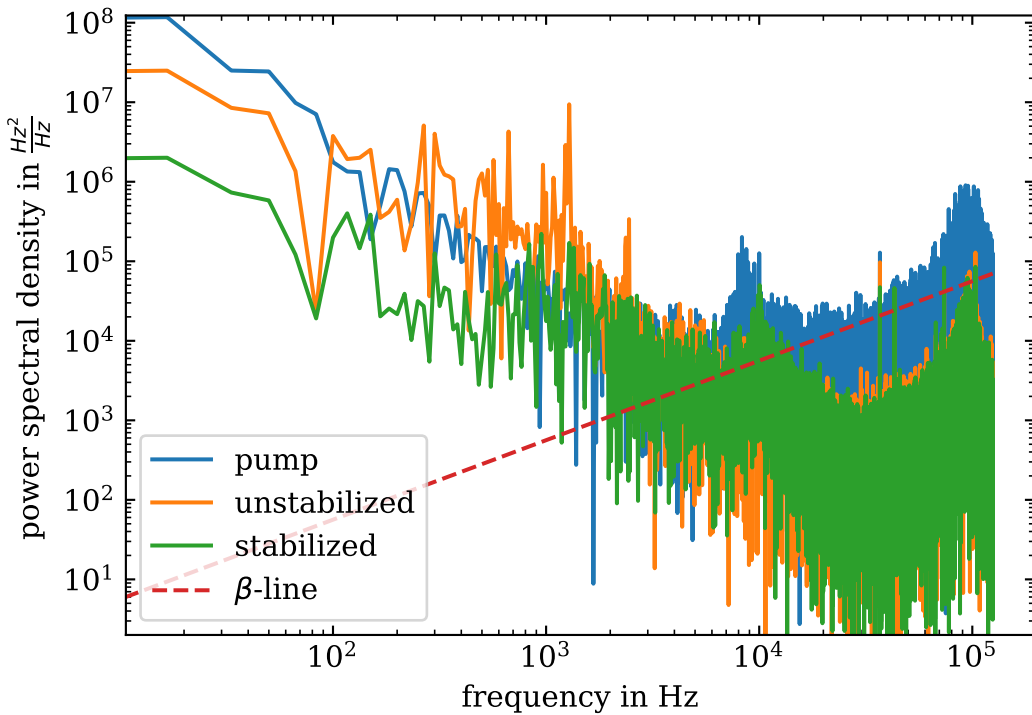


Figure 3.6: Power spectral density of the pump source, the orange light unstabilized and stabilized, and the β separation line separating the components influencing the linewidth from those not influencing. Only frequency components with a value above the β line contribute to the linewidth.

3 kHz. Some structures are, however, similar. Among them are a very narrow peak at 40 kHz, and another large one at 100 kHz. At 10 kHz is no peak for the unstabilized output.

Up to almost 1 kHz, the stabilized output's PSD is ten times lower than the unstabilized one. At 70 Hz, however, they match. Up to 10 kHz the stabilized PSD remains better, but by a decreasing amount, afterwards they are almost identical. An improvement above 20 kHz cannot be expected with the current stabilization setup, because that is the maximum usable bandwidth of the seed laser's piezo tuning. Luckily, the unstabilized output's PSD is below the β separation line for almost all frequency components above 10 kHz such that there is almost no need for stabilization above that frequency. At 10 kHz is a peak for the stabilized output, but not the unstabilized one. It is probably caused by the stabilization, for the Argos system has the same peak for some PID values, too.

3.6 Comparison with the Current System

Having optimized the stabilization setup and analyzed the linewidth of our new laser system, we have to compare it to the currently used Argos system. The 21.9 kHz we measured appears to be an improvement over the Argos' 58 kHz.

That linewidth is, however, differently defined and measured. It is the full width at half maximum of the spectroscopically in Pr:YSO determined laser line

over 86 ms [5]. Two effects have to be taken in consideration with that measurement. First, radiative broadening increases the measured linewidth. Second, the result is a convolution of the laser linewidth with itself, increasing the linewidth as well. Because of all these reasons, the measured linewidths cannot be compared. The setup necessary for that spectroscopy is more complicated thus we were not able to do it with the new laser system for this work.

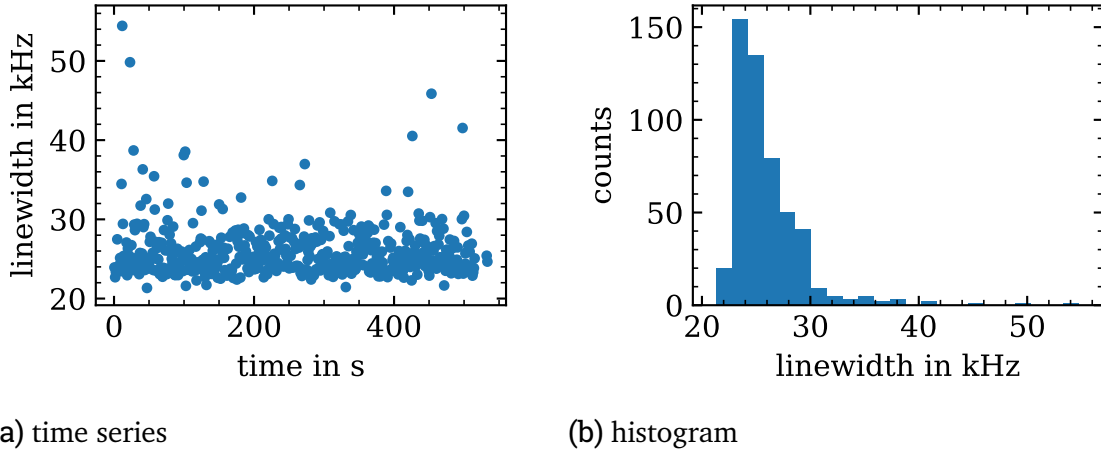


Figure 3.7: Series of linewidth measurements of the Aculight Argos System. Sub-figure (a) shows the linewidth over time and (b) the corresponding histogram. The average linewidth is 26 kHz with a standard deviation of 3.8 kHz.

The Eagle Eye measurement is simple to setup and we have recent measurement data for the Argos system, shown in figure 3.7. The average linewidth is 26 kHz with a standard deviation of 3.8 kHz. This linewidth is a lot smaller than the 58 kHz measured spectroscopically for the same system, but the latter is the full width at half maximum, while the first is the standard deviation of the frequency distribution. For a Gaussian distribution with a standard deviation of 26 kHz, which has both values and is similar to the Lorentzian of the spectroscopic measurement, the full width at half maximum is 61.2 kHz which is close to the 58 kHz.

Nevertheless, the two measurement techniques have too large systematic differences to compare their results for different systems. The Eagle Eye measurements were the same for both systems, thus these results can be compared. The average linewidth of the new system of 21.9 kHz is smaller than the Argos' linewidth of 26 kHz, but the standard deviation of 2.5 kHz and 3.8 kHz respectively does not allow a clear decision that the new system is better. Nevertheless, the new system reaches a similar linewidth.

The PSD reveals a few differences. Figure 3.8 shows the PSD of the new system and the Argos system in comparison. Both measurements took 60 ms. Up to 80 Hz, the new system has a power spectral density several times lower than the Argos' one. Afterwards they are comparable and above 600 Hz the Argos system is slightly better. Interestingly, the Argos system is more linear, while the new system has two broad peaks. One is around 1 kHz and the other one at 10 kHz. Sometimes, depending on to the PID values, the Argos system has the peak at 10 kHz as well, such that it is most probably caused by the stabilization system.

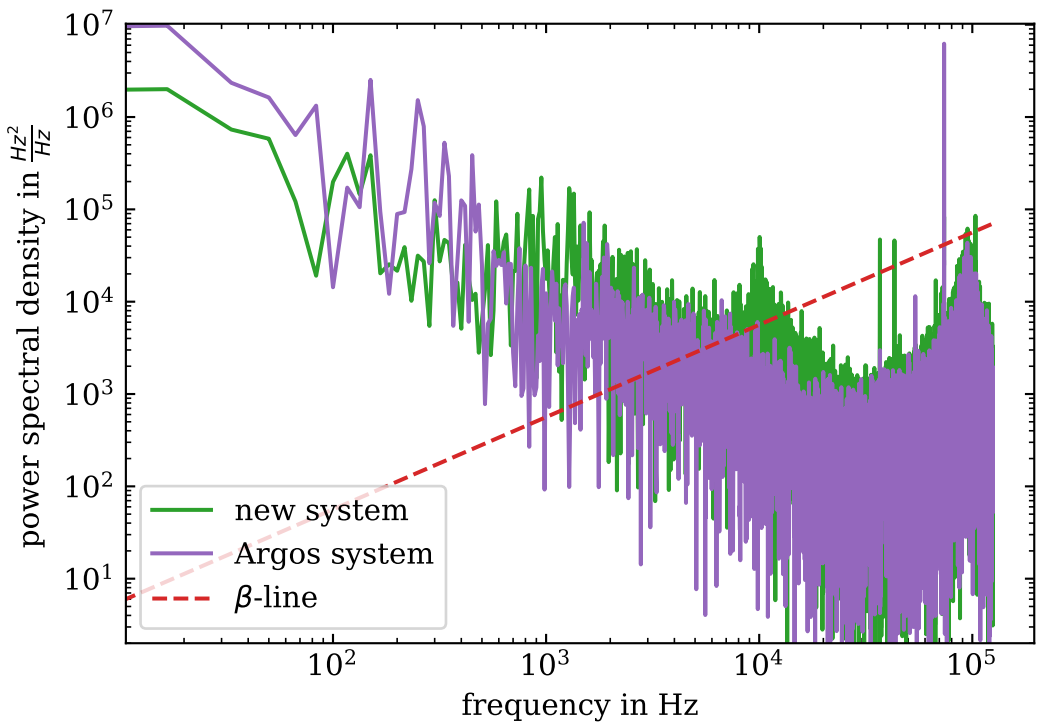


Figure 3.8: Power spectral density in comparison between our new laser system and Aculight's Argos system.

The comparable linewidths of the Argos system and the new system show, that it is possible to build an optical parametric oscillator at 606 nm partially with off-the-shelf components and achieve the performance of a commercially available product. It also shows, that the optical parametric oscillator was not the limiting part of the whole stabilization setup, because the result does not depend on which one was used.

Conclusion and Outlook

We set out to create a narrowband continuous wave source of coherent light at 606 nm for light storage experiments in praseodymium doped yttrium orthosilicate in order to replace the currently used Argos system. The setup we designed uses the nonlinear optical processes of optical parametric oscillation and sum frequency generation in order to convert coherent light at a wavelength of 1064 nm to 606 nm. In an output wavelength range of 605.5 nm to 607.5 nm, we reach an output power around 1 W. That is sufficient for the light storage experiments, where we need light at 605.982 nm with at least 0.5 W.

Although not part of the initial design goal, the setup can, with a different crystal, output light in the wavelength range of 3970 nm to 4500 nm. In this case, only the nonlinear process of optical parametric oscillation is used, whose idler is the output. These wavelengths are handy for spectroscopy of certain molecules, for example carbon dioxide [27]. Therefore, this alternative setup can be used for another project of our group.

Other output wavelength ranges should be possible, too. Only the cavity mirrors and the crystal need to be changed. The rest of the setup works for any optical parametric oscillator pumped at 1064 nm, because the design does not depend on the wavelength. The only requirement is, that the crystal is 50 mm long, made from PPLN, and the refractive index of the resonant signal is similar enough to the one at 1408 nm, that the cavity eigenmode remains the same. The glued in mirror prevents a simple mirror swap, instead, a second cavity block has to be manufactured. A design change without a glued in mirror would remove the need for a dedicated cavity block for each mirror set.

For the light storage experiments, the orange light has to be narrowband. Without acoustic decoupling or active stabilization, the linewidth of our system is almost 1 MHz. The linewidth of all our measurements is the standard deviation of the frequency fluctuation over 100 ms. Sonic waves increase the linewidth, especially if their frequencies are between 50 Hz and 4 kHz. A simple cardboard box for acoustic insulation reduced the linewidth to 348 kHz. Using a more stable pump source seed laser, the linewidth is reduced further to 260 kHz. A more elaborate acoustic box, lined with acoustic insulation foam, around the laser system reduces the linewidth to a mere 35 kHz.

An active stabilization setup using the Pound-Drever-Hall scheme proved to be effective for a linewidth reduction, even without acoustic insulation. With optimized settings of the stabilization setup, the average linewidth is 21.9 kHz with a standard deviation of 2.5 kHz. The power spectral density shows peaks at noise frequencies of 1 kHz and just below 10 kHz. Further improvements might try to reduce those. The Argos system does not have those peaks, but has more noise at lower frequencies such, that its average linewidth is 26 kHz with the same measurement method and a standard deviation of 3.8 kHz. Consequently,

Conclusion and Outlook

the new system is neither significantly better nor worse than the Argos system.

A spectroscopic measurement of the linewidth has still to be done for the new system. The current measurement system calculates the standard deviation of the frequency, interprets power fluctuations as frequency change, and cannot resolve a linewidth below 20 kHz. We are already close to that limit such that a spectroscopy is needed in order to measure the linewidth reliably.

Further improvements of the stabilization or laser system might increase the advantage of the new system over the Argos system, because the new system can be improved more easily than the commercial system. The new system features larger mirrors, an adjustable cavity, and more easily adjustable pump mirrors. Most importantly, we have the design data which allows us to either change details precisely or manufacture elements with a changed design.

Better passive stabilization might improve the linewidth. On one hand the acoustic insulation against sonic waves in air could be improved. On the other hand, acoustic decoupling of the system from the optical table and a vacuum housing could be tried. Our design data enables us to alter the design of the cavity block in order to match the vacuum housing.

The active stabilization did already reduce the linewidth, but not as much as expected, for Mhibik *et al.* reached a linewidth of less than 1 kHz over 1 s for an OPO with intracavity SHG [8]. The seed laser seems to be able to suppress noise sufficiently, because most of the noise relevant for the linewidth is below 10 kHz which is inside the seed laser tuning bandwidth. Neither does the OPO limit the linewidth, it seems, because both devices, the Argos system and the new system, perform the same. Two elements of the stabilization remain to test: the reference cavity and the DigiLock controller. The latter is a state of the art commercial product, but the former was made by our group and might be not as good as hoped for [7]. First, the finesse of our reference cavity was calculated to 3140, compared to 3000 of Mhibik *et al.*, but it might actually be worse. Second, the reference cavity might not be mechanically stable enough. A new reference cavity could alleviate both points and thus provide a better frequency reference.

Erklärung zur Abschlussarbeit gemäß §22 Abs. 7 und §23 Abs. 7 APB der TU Darmstadt

Hiermit versichere ich, Benedikt Moneke, die vorliegende Masterarbeit ohne Hilfe Dritter und nur mit den angegebenen Quellen und Hilfsmitteln angefertigt zu haben. Alle Stellen, die Quellen entnommen wurden, sind als solche kenntlich gemacht worden. Diese Arbeit hat in gleicher oder ähnlicher Form noch keiner Prüfungsbehörde vorgelegen.

Mir ist bekannt, dass im Fall eines Plagiats (§38 Abs. 2 APB) ein Täuschungsversuch vorliegt, der dazu führt, dass die Arbeit mit 5,0 bewertet und damit ein Prüfungsversuch verbraucht wird. Abschlussarbeiten dürfen nur einmal wiederholt werden.

Bei der abgegebenen Thesis stimmen die schriftliche und die zur Archivierung eingereichte elektronische Fassung gemäß §23 Abs. 7 APB überein.

Bei einer Thesis des Fachbereichs Architektur entspricht die eingereichte elektronische Fassung dem vorgestellten Modell und den vorgelegten Plänen.

Darmstadt, 3. September 2020

B. Moneke

Bibliography

- [1] P. Jobez *et al.* *Towards Highly Multimode Optical Quantum Memory for Quantum Repeaters*. Physical Review A **93**, 1–9 (2016).
- [2] G. Heinze, C. Hubrich, and T. Halfmann. *Stopped Light and Image Storage by Electromagnetically Induced Transparency up to the Regime of One Minute*. Physical Review Letters **111**, 033601,1–5 (July 2013).
- [3] M. Afzelius, C. Simon, H. de Riedmatten, and N. Gisin. *Multimode Quantum Memory Based on Atomic Frequency Combs*. Physical Review A **79**, 1–9 (2009).
- [4] M. Nilsson, L. Rippe, S. Kröll, R. Klieber, and D. Suter. *Hole-Burning Techniques for Isolation and Study of Individual Hyperfine Transitions in Inhomogeneously Broadened Solids Demonstrated in $Pr^{3+}:Y_2SiO_5$* . Physical Review B **70**, 1–11 (2004).
- [5] B. Moneke. *Laserfrequenzstabilisierung mit AOM für atomare Frequenzkämme in $Pr^{3+}:Y_2SiO_5$* . Bachelor-Thesis (TU Darmstadt, Aug. 2018).
- [6] R. A. Akhmedzhanov *et al.* *Atomic Frequency Comb Memory in an Isotopically Pure $i^{43}Nd^{3+}:Y^7LiF_4$ Crystal*. Laser Physics Letters **13**, 015202 (2016).
- [7] S. R. Mieth. *Preserving Atomic Coherences for Light Storage in $Pr^{3+}:Y_2SiO_5$ Driven by an OPO Laser System*. Dissertation (TU Darmstadt, 2016).
- [8] O. Mhibik, D. Pabœuf, C. Drag, and F. Bretenaker. *Sub-kHz-Level Relative Stabilization of an Intracavity Doubled Continuous Wave Optical Parametric Oscillator Using Pound-Drever-Hall Scheme*. Optics Express **19**, 18049–18057 (Sept. 2011).
- [9] N. N. Ledentsov *et al.* *Room-Temperature Yellow-Orange (In,Ga,Al)P–GaP Laser Diodes Grown on (N11) GaAs Substrates*. Optics Express **26**, 13985–13994 (May 2018).
- [10] S. Luo *et al.* *Power Scaling of Blue-Diode-Pumped $Pr:YLF$ Lasers at 523.0, 604.1, 606.9, 639.4, 697.8 and 720.9 nm*. Optics Communications **380**, 357–360 (Dec. 2016).
- [11] Spectra Physics. *Matisse 2*. <https://www.spectra-physics.com/products/tunable-lasers/matisse>. Accessed 02.09.2020.
- [12] D. Meschede. *Optik, Licht und Laser* Third (Vieweg + Teubner, Wiesbaden, 2008).
- [13] A. V. Smith. *SNLO Nonlinear Optics Code*. AS-Photonics. Albuquerque, NM.
- [14] G. Moore and K. Koch. *Optical Parametric Oscillation with Intracavity Sum-Frequency Generation*. IEEE Journal of Quantum Electronics **29**, 961–969 (Mar. 1993).

- [15] O. Mhibik, T.-H. My, D. Pabœuf, F. Bretenaker, and C. Drag. *Frequency Stabilization at the Kilohertz Level of a Continuous Intracavity Frequency-Doubled Singly Resonant Optical Parametric Oscillator*. Optics Letters **35**, 2364–2366 (July 2010).
- [16] W. R. Bosenberg, A. Drobshoff, J. I. Alexander, L. E. Myers, and R. L. Byer. *93% Pump Depletion, 3.5-W Continuous-Wave, Singly Resonant Optical Parametric Oscillator*. Optics Letters **21**, 1336–1338 (Sept. 1996).
- [17] A. V. Smith. *Crystal Nonlinear Optics with SNLO Examples* (AS-Photonics, Albuquerque, 2018).
- [18] G. New. *Introduction to Nonlinear Optics* (Cambridge University Press, Cambridge ; New York, 2011).
- [19] W. Demtröder. *Experimentalphysik. 2: Elektrizität und Optik* Sixth (Springer Spektrum, Berlin Heidelberg, 2013).
- [20] J. S. Otto. *Aufbau und Charakterisierung eines optisch parametrischen Verstärkers für mittel-infrarote ns-Pulse*. Master-Thesis (TU Darmstadt, Jan. 2018).
- [21] Sirah. *Eagle Eye*. <http://www.sirah.com/tools/eagleeye/unit>. Accessed 31.07.2020.
- [22] G. Di Domenico, S. Schilt, and P. Thomann. *Simple Approach to the Relation between Laser Frequency Noise and Laser Line Shape*. Applied Optics **49**, 4801–4807 (Sept. 2010).
- [23] A. Ly, B. Szymanski, and F. Bretenaker. *Frequency Stabilization of the Non Resonant Wave of a Continuous-Wave Singly Resonant Optical Parametric Oscillator*. Applied Physics B **120**, 201–205 (Aug. 2015).
- [24] F. Beil. *Kohärente optische Datenverarbeitung in einem seltenerd-dotierten Festkörper*. Dissertation (TU Darmstadt, Nov. 2010).
- [25] E. D. Black. *An Introduction to Pound–Drever–Hall Laser Frequency Stabilization*. American Journal of Physics **69**, 79–87 (Jan. 2001).
- [26] NKT Photonics. *Koheras ADJUSTIK Product Guide*. <https://www.nktphotonics.com/-wp-content/uploads/sites/3/2020/01/koheras-adjustik-product-guide-20200122-r01.pdf?1597240362>. Accessed 13.08.2020.
- [27] National Institute of Standards and Technology. *Carbon Dioxide*. <https://webbook.nist.gov/cgi/inchi?ID=C124389&Type=IR-SPEC&Index=1#IR-SPEC>. Accessed 31.08.2020.